Meteoritics & Planetary Science 39, Nr 3, 481–498 (2004)
Abstract available online at http://meteoritics.org

Exposure history and terrestrial ages of ordinary chondrites from the Dar al Gani region, Libya

K. C. WELTEN,[1*] K. NISHIIZUMI,[1] R. C. FINKEL,[2] D. J. HILLEGONDS,[2] A. J. T. JULL,[3] L. FRANKE,[4] and L. SCHULTZ[4]

[1]Space Sciences Laboratory, University of California, Berkeley, California 94720–7450, USA
[2]CAMS, Lawrence Livermore National Laboratory, Livermore, California 94550, USA
[3]NSF Arizona AMS Facility, University of Arizona, Tucson, Arizona 85721, USA
[4]Max-Planck-Institut für Chemie, Postfach 3060, D-55020 Mainz, Germany
*Corresponding author. E-mail: kcwelten@uclink4.berkeley.edu

(Received 12 December 2003; revision accepted 6 January 2004)

Abstract–We measured the concentrations of noble gases in 32 ordinary chondrites from the Dar al Gani (DaG) region, Libya, as well as concentrations of the cosmogenic radionuclides ^{14}C, ^{10}Be, ^{26}Al, ^{36}Cl, and ^{41}Ca in 18 of these samples. Although the trapped noble gases in five DaG samples show ratios typical of solar or planetary gases, in all other DaG samples, they are dominated by atmospheric contamination, which increases with the degree of weathering. Cosmic ray exposure (CRE) ages of DaG chondrites range from ~1 Myr to 53 Myr. The CRE age distribution of 10 DaG L chondrites shows a cluster around 40 Myr due to four members of a large L6 chondrite shower. The CRE age distribution of 19 DaG H chondrites shows only three ages coinciding with the main H chondrite peak at ~7 Myr, while seven ages are <5 Myr. Two of these H chondrites with short CRE ages (DaG 904 and 908) show evidence of a complex exposure history. Five of the H chondrites show evidence of high shielding conditions, including low $^{22}Ne/^{21}Ne$ ratios and large contributions of neutron-capture ^{36}Cl and ^{41}Ca. These samples represent fragments of two or more large pre-atmospheric objects, which supports the hypothesis that the high H/L chondrite ratio at DaG is due to one or more large unrecognized showers.

The ^{14}C concentrations correspond to terrestrial ages <35 kyr, similar to terrestrial ages of chondrites from other regions in the Sahara but younger than two DaG achondrites. Despite the loss of cosmogenic ^{36}Cl and ^{41}Ca during oxidation of metal and troilite, concentrations of ^{36}Cl and ^{41}Ca in the silicates are also consistent with ^{14}C ages <35 kyr. The only exception is DaG 343 (H4), which has a ^{41}Ca terrestrial age of 150 ± 40 kyr. This old age shows that not only iron meteorites and achondrites but also chondrites can survive the hot desert environment for more than 50 kyr. A possible explanation is that older meteorites were covered by soils during wetter periods and were recently exhumed by removal of these soils due to deflation during more arid periods, such as the current one, which started ~3000 years ago.

Finally, based on the $^{26}Al/^{21}Ne$ and $^{10}Be/^{21}Ne$ systematics in 16 DaG meteorites, we derived more reliable estimates of the $^{10}Be/^{21}Ne$ production rate ratio, which seems more sensitive to shielding than was predicted by the semi-empirical model of Graf et al. (1990) but less sensitive than was predicted by the purely physical model of Leya et al. (2000).

INTRODUCTION

In the past two decades, thousands of meteorites have been recovered from hot deserts in Australia, North Africa, and Oman. These new meteorite collections have greatly increased the availability of many different meteorite types, including lunar and martian meteorites. One of the main meteorite concentration surfaces in the Sahara is the Dar al Gani (DaG) plateau in central Libya, which covers a total area of ~8,000 km^2. In the past decade, more than 1000 meteorites have been recovered from this region. The geological setting, pairing of meteorites, and recovery density of the DaG field are described in Schlüter et al. (2002).

So far, only a few terrestrial ages are known for DaG meteorites, i.e., 60 ± 20 kyr for the DaG 476 shergottite shower (Nishiizumi et al. 2001a) and 80 ± 20 kyr for the lunar meteorite DaG 262 (Nishiizumi et al. 1998). However, based on the long terrestrial ages of 300–500 kyr for two achondrites from Oman (Nishiizumi et al. 2001b, 2002)—compared to terrestrial ages of <40 kyr for chondrites (Jull et al. 2002)—it was recently suggested that metal-poor achondrites might survive desert environments much longer than metal-rich meteorites, such as ordinary chondrites. The terrestrial ages of the two DaG achondrites may, therefore, not be representative of the majority of the DaG meteorite collection, of which more than 90% are ordinary chondrites.

In this work, we report concentrations and isotopic composition of He, Ne, and Ar, as well as the concentrations of ^{84}Kr and ^{132}Xe in 32 ordinary chondrites from the DaG area. In addition, we report concentrations of the cosmogenic radionuclides ^{14}C (half-life = 5,730 yr), ^{41}Ca (1.04×10^5 yr), ^{36}Cl (3.01×10^5 yr), ^{26}Al (7.05×10^5 yr), and ^{10}Be (1.5×10^6 yr) in 18 of these samples. We discuss the thermal history and cosmic ray exposure (CRE) history of these meteorites as well as their pre-atmospheric size and possible pairings. In addition, we determine the terrestrial ages of 18 DaG meteorites and evaluate the effects of the hot desert environment on the noble gas and radionuclide records. Finally, we will use the ^{10}Be/^{21}Ne and ^{26}Al/^{21}Ne ratios in selected DaG samples to evaluate the shielding dependence of the ^{10}Be/^{21}Ne production rate ratio.

EXPERIMENTAL PROCEDURES

Samples

We selected 32 ordinary chondrites from the DaG area for noble gas analysis. To avoid pairing as much as possible, we selected meteorites from many different locations in the DaG area, up to ~140 km apart (Fig. 1). In addition, we selected meteorites of different chemical and petrologic classification, shock grade and degree of weathering. One exception to this sampling strategy is the selection of four L6 chondrites (DaG 328, 457, 458, 757) that were identified to be part of a large pairing group. We also selected two L6 chondrites (DaG 341 and 906) that may be part of a small pairing group (Schlüter et al. 2002). The selected samples include 19 H, 10 L, 1 L/LL, and 2 LL chondrites, ranging from petrologic type 3 to type 6 (Table 1). The shock grade ranges from S1 to S6 according to the shock classification of Stöffler et al. (1991). The weathering grade of the selected meteorites ranges from W0 (no signs of oxidation of metal or troilite) to W5 (complete oxidation of metal and troilite as well as beginning alteration of mafic silicates) according to the weathering scale of Wlotzka (1993). For the radionuclide measurements, we selected 18 of the 32 samples measured for noble gases. The noble gas exposure age, contents of radiogenic ^{4}He and ^{40}Ar, as well as classification and find location were used to avoid possible pairings.

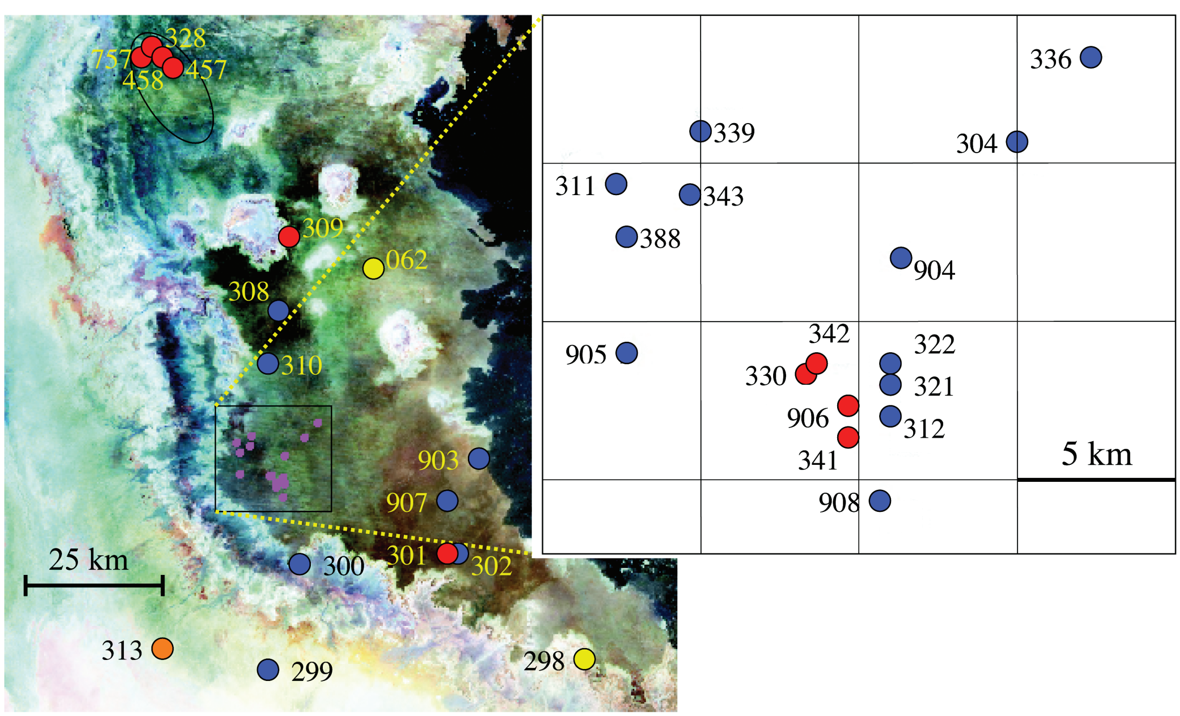

Fig. 1. Distribution of selected samples projected on a satellite image (Landsat 7, USGS) of the DaG region, in central Libya. The light-colored area on the west side represents Jurassic and Cretaceous clastic sediments, while the dark area on the east side represents the basaltic complex of the Haruj al Aswad. Blue dots represent H, red dots L, orange dots L/LL, and yellow dots LL chondrites. The oval shape in the North part of DaG represents a large strewnfield of L6 chondrites, including DaG 328, 457, 458, and 757. The central part of the DaG region, which shows the highest meteorite concentration, is enlarged 5× to show the distribution of samples selected from this area.

Table 1. Noble gas concentrations (in 10^{-8} cm^3 STP/g) and isotopic ratios in 45 samples of 32 different DaG meteorites.[a]

DaG	Type	^{3}He	^{4}He	^{20}Ne	^{21}Ne	^{22}Ne	^{36}Ar	^{38}Ar	^{40}Ar	$^{3}He/^{21}Ne$	$^{22}Ne/^{21}Ne_c$	^{84}Kr	^{132}Xe	$^{132}Xe/^{84}Kr$
299	H4, S2, W3	50.1	1527	10.70	8.87	10.43	11.06	2.91	7403	5.65	1.151	0.29	0.055	0.19
300	H3–6, S2, W1	21.3	1167	3.66	3.54	4.30	6.64	1.86	4469	6.03	1.213	0.07	0.071	1.03
302	H5, S2, W5	46.3	1395	10.63	11.17	11.95	10.95	3.03	7613	4.15	1.064	0.52	0.088	0.17
304-1	H6, S3, W4	1.15	897	2.58	0.34	0.55	15.19	2.94	8932	3.40	*1.05*	0.59	0.076	0.13
304-2		1.13	723	2.54	0.33	0.53	13.58	2.61	8508	3.41	*1.05*	0.52	0.075	0.14
304-3		1.06	866	2.53	0.35	0.58	21.06	4.01	11262	3.05	*1.05*	–	–	–
304-4		0.93	670	1.70	0.32	0.47	16.03	3.07	9607	2.93	*1.05*	–	–	–
308	H6, S3, W2	2.92	595	2.31	1.17	1.35	6.50	1.36	5093	2.49	1.041	0.19	0.024	0.13
310	H5/6, S3, W2	33.5	1578	7.92	7.97	8.55	8.37	2.24	6278	4.19	1.062	0.33	0.045	0.14
311-1	H6, S3, W3	6.80	1210	2.31	1.64	1.80	8.30	1.68	6479	4.15	1.043	0.31	0.055	0.18
311-2		4.04	1005	3.82	1.63	1.94	10.33	2.15	7583	2.48	1.041	0.33	0.039	0.12
311-3		7.04	1234	1.71	1.61	1.71	3.37	0.79	6174	4.37	1.045	0.17	0.054	0.32
312	H6, S3, W2	40.2	400	8.83	9.35	10.49	1.98	1.31	774	4.30	1.121	0.07	0.015	0.21
321-1	H5, S3, W3	6.16	595	4.48	2.37	2.82	1.50	0.49	2440	2.60	1.111	0.08	0.031	0.40
321-2		5.30	546	4.16	2.20	2.62	1.47	0.48	2397	2.41	1.111	0.07	0.026	0.37
322	H4, S2, W2	30.4	1332	4.75	4.05	5.01	5.78	1.67	6548	7.51	1.221	0.07	0.026	0.37
336	H5/6, S2, W4	5.33	1317	1.43	0.95	1.13	6.51	1.33	7196	5.62	1.138	0.44	0.070	0.16
339	H5, S3, W3	3.29	596	8.83	1.57	2.45	5.64	1.23	2656	2.10	*1.18*	0.28	0.048	0.17
343-1	H4, S2, W4	6.33	1346	1.03	0.81	1.07	4.41	0.93	6527	7.82	1.304	0.19	0.063	0.34
343-2		6.69	1370	1.11	0.82	1.07	2.87	0.49	6902	8.17	1.273	–	–	–
388	H5/6, S2, W5	44.6	1429	10.51	11.41	12.31	2.74	1.55	4929	3.89	1.077	0.14	0.035	0.26
903-1	H3–6, S2, W3	20.9	8970	56.85	3.97	9.07	4.63	1.31	8585	5.27	*1.11*	0.11	0.037	0.34
903-2		16.0	5104	35.19	3.55	6.97	4.02	1.18	7420	4.51	*1.11*	0.15	0.045	0.29
904-1	H6, S2, W3	1.11	794	0.35	0.39	0.42	1.06	0.22	4763	2.85	1.077	0.05	0.021	0.43
904-2		1.16	874	0.36	0.38	0.41	1.27	0.26	4868	3.05	1.071	0.06	0.021	0.34
905	H6, S3, W3	2.81	1088	0.83	0.86	0.89	1.71	0.37	5320	3.27	*1.05*	0.06	0.020	0.34
907	H6, S1, W3	22.7	1919	4.27	4.61	5.03	1.75	0.90	6051	4.92	1.090	0.10	0.016	0.17
908-1	H6, S4, W1	0.22	30	2.11	0.25	0.46	5.95	1.15	1690	0.86	*1.08*	0.09	0.010	0.11
908-2		0.22	41	1.99	0.30	0.50	4.58	0.85	1334	0.74	*1.08*	0.09	0.009	0.10
301	L6, S3, W5	31.2	234	10.19	9.31	9.93	15.63	3.79	4246	3.35	1.060	0.59	0.156	0.27
309	L6, S4, W2	13.6	763	3.61	2.22	2.84	6.69	1.55	7396	6.14	1.218	0.20	0.022	0.11
328	L6, S3, W1	66.4	627	13.94	15.51	16.40	2.38	2.30	1638	4.28	1.056	0.01	0.007	~1.0
330	L5, S2, W3	12.5	1098	2.47	2.52	2.91	12.73	2.29	8380	4.96	1.154	0.80	0.122	0.15
341	L6, S3, W3	17.7	761	3.07	3.33	3.85	2.45	0.78	6169	5.33	1.157	0.18	0.045	0.25
342	L5–6, S2, W3	58.2	1437	15.69	17.10	18.31	3.80	2.06	4784	3.40	1.069	0.07	0.025	0.34
457-1	L6, S6, W1	63.9	865	13.89	15.35	16.35	4.43	2.23	1868	4.16	1.064	0.01	0.007	~0.7
457-2		66.4	619	13.60	15.11	16.49	2.52	2.17	2062	4.39	1.091	0.02	0.009	0.39
458	L6, S4, W1	72.4	663	15.08	16.66	17.78	2.82	2.38	1613	4.34	1.066	0.002	0.002	~1.0
757	L6, S3/4, W1	43.2	574	9.93	10.90	11.72	2.54	1.51	1892	3.97	1.074	0.008	0.008	~1.0
906	L6, S3, W2	8.30	1374	1.85	0.87	1.22	6.25	1.25	6048	9.54	1.296	0.18	0.020	0.11
313	L/LL3, S3, W2	15.1	1364	6.82	3.48	4.40	39.93	7.97	6249	4.34	1.146	0.73	0.397	0.55
298	LL4, S3, W0	88.5	1968	16.60	17.97	19.83	1.82	2.15	6289	4.92	1.104	–	–	–
062-1	LL5–6, S3, W1	19.2	1216	3.18	3.39	3.87	10.92	2.32	7826	5.65	1.142	0.88	0.158	0.21
062-2		20.7	1358	3.59	3.69	4.19	2.11	0.80	5868	5.61	1.136	–	–	–
062-3		18.9	1479	3.44	3.72	4.20	1.99	0.92	6146	5.08	1.128	0.13	0.026	0.21

[a]S1–S6 = shock stage (Stöffler et al. 1991); W0–W5 = weathering grade (Wlotzka 1993); cosmogenic $^{22}Ne/^{21}Ne$ ratios with large uncertainties due to corrections for trapped Ne are shown in italics.

Noble Gas Measurements

Concentrations and isotopic ratios of He, Ne, and Ar as well as concentrations of ^{84}Kr and ^{132}Xe were measured in chips of ~100 mg at the Max Planck Institute, as described previously (Scherer et al. 1998). Noble gas results for several meteorites (DaG 062, 298–302, 304, 308–311, 313) were previously reported in Scherer et al. (1998, 2000) and Patzer et al. (1999).

The measured noble gas concentrations, given in Table 1, are a mixture of trapped, radiogenic, and cosmogenic components. Since the trapped Ne in most samples is dominated by atmospheric Ne, we assume $(^{20}Ne/^{22}Ne)_{tr}$ = 9.8 for samples with $(^{20}Ne/^{36}Ar)_{tr}$ <1, except for DaG 300 and 313, which contain planetary Ne, for which we assume $(^{20}Ne/^{22}Ne)_{tr}$ = 8.4. For samples with $(^{20}Ne/^{36}Ar)_{tr}$ >1, we assume $(^{20}Ne/^{22}Ne)_{tr}$ = 12.0, corresponding to solar Ne. In addition, we assume a ^{36}Ar/^{38}Ar ratio of 5.32 (Scherer et al. 1998) and a ^{40}Ar/^{36}Ar ratio of 250 for trapped atmospheric Ar (Welten et al. 2003). The latter value is ~15% lower than the atmospheric ratio of 296 but is in better agreement with the experimental data. The uncertainty in the trapped ^{40}Ar/^{36}Ar ratio affects the concentration of radiogenic ^{40}Ar by <10% for most samples, except for DaG 301 and 908, in which >80–90% of the ^{40}Ar is due to atmospheric contamination. For meteorites with planetary Ar (DaG 313), we assume a ^{40}Ar/^{36}Ar ratio of <1 for the trapped component (Marti 1967). In addition, some meteorites that were exposed under high shielding may contain a small contribution of ^{36}Ar from the decay of neutron-capture ^{36}Cl, but this component is generally small compared to the contribution of trapped ^{36}Ar.

For the cosmogenic component, we assume ratios of $(^{4}He/^{3}He)_c = 6$ for He (Alexeev 1998), $(^{20}Ne/^{22}Ne)_c = 0.84$ for Ne, and $(^{36}Ar/^{38}Ar)_c = 0.67$ for Ar (Scherer et al. 1998). The concentration of cosmogenic ^{38}Ar is difficult to determine for some DaG meteorites due to large amounts of trapped Ar: in seven samples >90% of the measured ^{38}Ar is trapped Ar, in most cases, atmospheric contamination. The concentration of cosmogenic ^{21}Ne is more reliable since the amount of trapped ^{21}Ne is usually negligible (<1%). Corrections for trapped ^{22}Ne are <10% for meteorites with ^{20}Ne/^{22}Ne ratios <1.7 but become more significant for samples with ^{20}Ne/^{22}Ne ratios >1.7, resulting in a less-precise cosmogenic ^{22}Ne/^{21}Ne ratio (which otherwise has an uncertainty of ~1%). Four samples (DaG 304, 339, 903, and 908) show elevated ^{20}Ne/^{22}Ne ratios of 3.6–5.3. For DaG 339 and 908, we adopted the corrected $(^{22}Ne/^{21}Ne)_c$ ratios of 1.18 ± 0.03 and 1.08 ± 0.03, respectively (Table 1). For DaG 304 and 903, we adopted the lower cut-off value of 1.05 and the average value of 1.11, respectively.

We calculated CRE ages from the cosmogenic ^{3}He, ^{21}Ne, and ^{38}Ar concentrations and production rate methods, which use the ^{22}Ne/^{21}Ne ratio as a shielding parameter (Nishiizumi et al. 1980; Eugster 1988). We lowered the ^{38}Ar production rate of Eugster (1988) by 13% as suggested by Schultz et al. (1991). The ^{21}Ne ages, given in Table 2, have typical uncertainties of 10% for meteorites with ^{22}Ne/^{21}Ne ratios >1.10, while the ages are less reliable for meteorites with low ^{22}Ne/^{21}Ne ratios, as will be discussed later. In contrast, the ^{3}He and ^{38}Ar ages have uncertainties >10% for all samples due to gas losses and uncertainties in the cosmogenic ^{38}Ar concentrations.

After correcting measured concentrations of ^{4}He and ^{40}Ar for cosmogenic ^{4}He and trapped ^{40}Ar, we determined U,Th-^{4}He and ^{40}K-^{40}Ar gas retention ages, assuming average concentrations of Th, U, and K in ordinary chondrites from Wasson and Kallemeyn (1988). These ages, shown in Table 2, have typical uncertainties of 10–20%, mainly due to uncertainties in the correction for trapped ^{40}Ar and to variations in concentrations of Th, U, and K.

Radionuclide Measurements

Cosmogenic ^{14}C was extracted from bulk meteorite samples of 80–570 mg using techniques described previously (Jull et al. 1989, 1990). Measurements of ^{14}C by accelerator mass spectrometry (AMS) were carried out at the University of Arizona. Uncertainties in the measured ^{14}C concentrations range from ~1% in samples with high ^{14}C to ~15% in samples with low ^{14}C. For measurements of ^{10}Be, ^{26}Al, ^{36}Cl, and ^{41}Ca, we crushed ~1 g of sample and separated the metal (if any). The stone fraction was homogenized, and an aliquot of 100–140 mg was used for radionuclide analyses. For one sample, DaG 908, we also measured radionuclide concentrations in 61.4 mg of the metal fraction. The stone fraction was dissolved together with carrier solutions, containing 3–5 mg of Be and Cl, in concentrated HF/HNO_3. After dissolution, aliquots of the dissolved samples were taken for chemical analysis by atomic absorption spectroscopy (AAS). To the remaining solution, a carrier solution containing 5–10 mg Al was added. The Be, Al, Cl, and Ca fractions were isolated using chemical separation methods described previously (Welten et al. 2000) and were purified and converted to BeO, Al_2O_3, AgCl, and CaF_2. Measurements of ^{10}Be, ^{26}Al, ^{36}Cl, and ^{41}Ca were carried out at the Lawrence Livermore National Laboratory AMS facility (Davis et al. 1990). The measured ^{10}Be/Be, ^{26}Al/Al, ^{36}Cl/Cl, and ^{41}Ca/Ca ratios were normalized to the following standards: an ICN (ICN Chemical & Radioisotope Division) ^{10}Be standard, NBS (National Bureau of Standards) ^{26}Al and ^{36}Cl standards (Nishiizumi et al. 1984; Sharma et al. 1990; Nishiizumi Forthcoming), and a ^{41}Ca standard (Nishiizumi et al. 2000). The measured radionuclide concentrations given in Table 3 include 1σ uncertainties of the AMS measurements but not the absolute uncertainties in the standards. The chemical composition of each sample is given in Table 4.

Table 2. Cosmic ray exposure ages (T_3, T_{21}, and T_{38} in Myr) and gas retention ages (T_4 and T_{40} in Gyr) based on concentrations (in 10^{-8} cm^3 STP/g) of cosmogenic ^3He, ^{21}Ne, and ^{38}Ar and radiogenic ^4He and ^{40}Ar. CRE ages are based on the production rates of Eugster (1988), while radiogenic ages are based on the chondritic U, Th, and K concentrations of Wasson and Kallemeyn (1988).[a]

DaG	$^{22}Ne/^{21}Ne_c$	^3He	^{21}Ne	^{38}Ar	T_3	T_{21}	T_{38}	T_3/T_{21}	^4He_r	T_4	$^{40}Ar_r$	T_{40}	T_4/T_{40}
H chondrites													
299	1.151	50.1	8.86	0.95	31.4	34.0	23.4	0.92	1226	3.55	4797	4.15	0.86
300	1.213	21.3	3.54	0.70	13.6	16.8	19.2	0.81	1039	3.18	2926	3.95	0.80
302	1.064	46.3	11.17	1.11	28.4	28.7	23.9	0.99	1117	3.34	5062	4.24	0.79
304	*1.05*	1.07	0.33	*0.07*	0.70	0.79	–	0.84	783	2.56	5472	4.37	0.59
308	1.041	2.92	1.17	0.15	*1.8*	2.6	3.2	0.68	577	1.99	3494	3.64	0.55
310	1.062	33.5	7.97	0.76	20.5	20.3	16.4	1.01	1377	3.81	4313	3.98	0.96
311	1.044	6.92	1.62	0.18	4.2	3.7	3.8	1.14	1180	3.47	4900	4.20	0.83
312	1.121	40.2	9.35	1.07	25.0	31.6	25.2	0.79	159	0.60	460	1.10	0.55
321	1.111	5.73	2.28	0.24	*3.6*	7.4	5.5	0.48	536	1.87	2087	2.86	0.65
322	1.221	30.4	4.05	0.67	19.4	19.6	18.7	0.99	1149	3.40	5216	4.29	0.79
336	1.138	5.33	0.95	0.12	3.3	3.4	2.9	0.97	1285	3.66	5589	4.41	0.83
339	*1.18*	3.29	1.54	0.20	*2.1*	6.6	5.1	0.32	576	1.99	1279	2.18	0.91
343	1.288	6.51	0.81	0.11	4.2	4.7	3.9	0.89	1319	3.72	5444	4.36	0.85
388	1.077	44.6	11.41	1.18	27.3	31.5	26.0	0.87	1163	3.43	4442	4.03	0.85
903	*1.11*	16.2	3.62	0.49	10.0	11.7	11.4	0.86	–[b]	–[b]	–[b]	–[b]	–[b]
904	1.075	1.14	0.38	0.02	*0.7*	1.0	0.5	0.66	827	2.68	4528	4.06	0.66
905	*1.05*	2.81	0.86	0.06	1.7	2.0	1.2	0.84	1071	3.24	4902	4.19	0.77
907	1.090	22.7	4.61	0.65	14.0	13.6	14.6	1.03	1783	4.32	5723	4.45	0.97
908	*1.08*	0.22	0.27	0.03	*0.14*	0.77	0.8	0.18	34	0.13	198	0.56	0.24
L and LL chondrites													
062	1.132	19.8	3.70	0.54	12.3	12.2	14.0	1.01	1300	3.68	5600	3.95	0.93
298	1.104	88.5	17.97	2.07	54.8	52.6	47.2	0.85	1437	3.90	6180	4.48	0.87
301	1.044	31.2	9.30	0.97	19.0	19.7	20.4	0.96	47	0.18	502	1.13	0.16
309	1.218	13.6	2.22	0.33	8.7	9.9	9.2	0.88	681	2.29	5780	4.37	0.52
313	1.146	15.1	3.47	0.53	9.5	12.1	13.4	0.78	1274	3.64	6235	4.50	0.81
328	1.056	66.4	15.51	2.12	40.6	35.4	45.1	1.15	229	0.86	1398	2.23	0.38
330	1.154	12.5	2.52	–	7.9	9.1	–	0.86	1023	3.14	5176	4.19	0.75
341	1.157	17.7	3.33	0.36	11.1	12.1	9.8	0.92	655	2.21	5619	4.32	0.51
342	1.069	58.2	17.09	1.54	35.7	41.9	36.1	0.85	1088	3.28	4091	3.80	0.86
457	1.078	65.1	15.23	1.77	40.0	39.3	38.9	1.02	351	1.28	1393	2.22	0.58
458	1.066	72.4	16.66	2.12	44.3	40.3	45.7	1.10	229	0.86	1263	2.10	0.41
757	1.074	43.2	10.90	1.18	26.6	27.5	25.8	0.96	315	1.16	1455	2.28	0.51
906	1.296	8.30	0.87	0.09	5.4	4.8	3.0	1.13	1324	3.73	4500	3.96	0.94

[a]Cosmogenic $^{22}Ne/^{21}Ne$ ratios with large uncertainties due to corrections for trapped Ne are shown in italics as are low ^3He ages due to loss of cosmogenic ^3He and ^{38}Ar concentrations and ages with large uncertainties due to large corrections (i.e., >90%) of trapped ^{38}Ar.
[b]Due to large amounts of solar gases in DaG 903, radiogenic gas concentrations and ages could not be calculated.

NOBLE GASES: THERMAL HISTORY, COSMIC RAY EXPOSURE HISTORY, AND EFFECTS OF TERRESTRIAL WEATHERING

Trapped Noble Gases

Most DaG samples contain significant amounts of trapped Ne, Ar, Kr, and Xe. The trapped $^{20}Ne/^{36}Ar$ ratios in most of these samples are <0.4, (averaging 0.13 ± 0.09), indicating that trapped Ne and Ar in these samples is dominated by atmospheric contamination (Fig. 1a). The only exception to this trend is DaG 313, an L/LL3 chondrite with a very high trapped ^{36}Ar concentration and a trapped $^{20}Ne/^{36}Ar$ ratio of ~0.1. The trapped gases in this unequilibrated meteorite are clearly dominated by planetary noble gases, as is also evident from the high ^{132}Xe concentration and high $^{132}Xe/^{84}Kr$ ratio (Marti 1967). In addition, three samples (DaG 321, 339, and 903) show elevated $(^{20}Ne/^{36}Ar)_{tr}$ ratios of 1.3–10.7, which indicate significant contributions of solar neon. The largest contribution of solar gases is found in DaG 903, an H3–6 chondrite regolith breccia, which also shows very high concentrations of ^4He as well as trapped ^{20}Ne. Based on a $^{20}Ne/^{36}Ar$ ratio of ~20 for the solar-gas-rich matrix of Fayetteville (Wieler et al. 1989), the ratio of 10.7 in DaG 903 indicates that ~99% of the trapped Ne and ~50% of the trapped Ar are solar. DaG 321 and 339 also show elevated $(^{20}Ne/^{36}Ar)_{tr}$ ratios

Table 3. Cosmogenic radionuclide concentrations (in dpm/kg.stone) and ^{14}C and ^{14}C-^{10}Be terrestrial ages (T, in 10^3 yr) of 18 DaG meteorites.

DaG	Type	^{14}C	T(^{14}C)	T($^{14}C/^{10}Be$)	^{10}Be	^{26}Al	^{36}Cl	^{36}Cl[a]	^{41}Ca	^{41}Ca[b]
304	H6	–	–	–	6.1 ± 0.1	29.6 ± 0.6	9.7 ± 0.2	44 ± 3	13.6 ± 0.6	74 ± 6
308	H6	5.1 ± 0.3	18.3 ± 1.4	–	13.7 ± 0.3	43.9 ± 0.9	9.9 ± 0.2	42 ± 3	10.5 ± 0.5	53 ± 5
311	H6	4.1 ± 0.6	20.1 ± 1.8	–	13.2 ± 0.3	39.5 ± 0.8	9.5 ± 0.2	42 ± 3	10.4 ± 0.6	55 ± 5
312	H6	2.8 ± 0.2	23.1 ± 1.5	22.0 ± 0.9	14.9 ± 0.3	37.2 ± 0.7	4.1 ± 0.1	19 ± 1	3.7 ± 0.2	20 ± 2
321	H5	6.3 ± 0.3	16.5 ± 1.4	16.5 ± 0.7	18.2 ± 0.4	49.1 ± 1.0	4.8 ± 0.1	21 ± 2	5.1 ± 0.5	26 ± 3
322	H4	34.4 ± 0.9	2.5 ± 1.3	1.0 ± 0.6	15.5 ± 0.3	43.6 ± 1.1	4.9 ± 0.1	21 ± 2	5.5 ± 0.3	28 ± 3
336	H5/6	2.3 ± 0.1	24.8 ± 1.4	26.2 ± 0.9	16.5 ± 0.3	46.2 ± 1.2	4.5 ± 0.1	22 ± 2	3.0 ± 0.3	17 ± 2
339	H5	15.2 ± 0.2	9.2 ± 1.3	8.4 ± 0.6	15.8 ± 0.3	45.3 ± 0.9	4.9 ± 0.1	22 ± 2	4.5 ± 0.2	24 ± 2
343	H4	1.1 ± 0.2	>31	>30	13.7 ± 0.3	34.9 ± 0.7	3.4 ± 0.1	14 ± 1	1.6 ± 0.3	9 ± 2
388	H5/6	2.3 ± 0.2	24.9 ± 1.5	24.9 ± 0.9	17.5 ± 0.4	47.2 ± 1.0	5.0 ± 0.1	22 ± 2	3.6 ± 0.3	19 ± 2
904	H6	1.6 ± 0.2	27.6 ± 1.6	–	5.1 ± 0.1	25.4 ± 0.5	12.2 ± 0.2	52 ± 4	18.5 ± 0.9	94 ± 8
907	H6	30.4 ± 0.2	3.5 ± 1.3	4.1 ± 0.7	21.0 ± 0.4	53.6 ± 1.1	5.8 ± 0.1	23 ± 2	4.1 ± 0.4	19 ± 2
908	H6	34.4 ± 0.2	2.5 ± 1.3	–	7.7 ± 0.4	40.1 ± 0.8	11.4 ± 0.2	40 ± 3	5.2 ± 0.4	22 ± 2
330	L5	25.9 ± 0.2	5.6 ± 1.3	4.6 ± 0.6	17.2 ± 0.3	49.2 ± 1.0	5.4 ± 0.1	20 ± 2	4.1 ± 0.3	18 ± 2
341	L6	24.7 ± 0.2	6.0 ± 1.3	5.4 ± 0.6	17.7 ± 0.4	47.2 ± 0.9	4.9 ± 0.1	19 ± 1	3.6 ± 0.3	17 ± 2
342	L5–6	14.6 ± 0.2	10.3 ± 1.3	10.4 ± 0.6	20.1 ± 0.4	53.5 ± 1.1	5.6 ± 0.1	20 ± 2	4.5 ± 0.7	19 ± 3
906	L6	8.5 ± 0.2	14.8 ± 1.3	13.2 ± 0.6	13.9 ± 0.3	36.9 ± 0.7	4.5 ± 0.1	17 ± 1	4.3 ± 0.3	19 ± 2
062	LL5–6	34.5 ± 0.3	3.9 ± 1.3	3.3 ± 0.6	19.7 ± 0.4	52.9 ± 1.1	7.5 ± 0.2	26 ± 2	5.7 ± 0.3	22 ± 2

[a]dpm/kg(Fe + 8Ca + 15K).
[b]dpm/kg(Fe + 6Ca) (see text).

Table 4. Elemental concentrations (in wt%), measured by atomic absorption spectrometry, in stone fraction of 18 DaG meteorites. The bulk content of unoxidized metal is indirectly derived from the measured concentrations of Fe + Ni in the stone fraction.

DaG	Type	Metal	Mg	Al	K	Ca	Fe	Ni
304	H6	0.0	12.4	1.19	0.11	1.34	23.8	1.2
308	H6	2.2	13.9	1.24	0.09	1.51	22.4	1.3
311	H6	0.0	13.3	1.17	0.09	1.47	24.1	1.6
312	H6	0.0	13.1	1.00	0.09	1.33	23.0	1.7
321	H5	3.2	14.0	1.09	0.09	1.43	21.7	1.5
322	H4	6.8	15.2	1.10	0.09	1.36	20.0	1.2
336	H5/6	0.0	13.1	1.10	0.11	1.16	24.2	1.1
339	H5	2.0	14.2	1.11	0.10	1.37	22.4	1.4
343	H4	5.8	14.0	1.12	0.11	1.46	20.6	1.1
388	H5/6	0.0	12.8	1.07	0.10	1.48	23.8	1.6
904	H6	1.1	14.0	1.09	0.10	1.52	22.8	1.5
907	H6	12.6	15.2	1.23	0.11	1.45	17.2	0.4
908	H6	18.0	17.4	1.49	0.09	1.73	13.0	0.6
330	L5	2.4	15.2	1.23	0.10	1.38	19.5	0.7
341	L6	<0.5	14.5	1.18	0.10	1.33	21.4	0.7
342	L5–6	5.1	15.2	1.19	0.10	1.50	17.8	0.6
906	L6	<0.5	14.6	1.02	0.09	1.51	21.1	1.2
062	LL5–6	1.5	15.5	1.17	0.10	1.43	19.6	1.1

(Fig. 2a), indicating that they contain a small contribution of solar gases, even though this is not apparent from their relatively low ^{4}He concentrations. The ratio of trapped $^{132}Xe/^{84}Kr$ ranges from 0.1–0.5 in most DaG samples (Fig. 2b), which is much closer to the value of dissolved $^{132}Xe/^{84}Kr$ = 0.073 in water (at 0 °C) than to the average planetary value of ~1.7 (Scherer et al. 1994). Higher $^{132}Xe/^{84}Kr$ ratios (combined with ^{132}Xe concentrations >10^{-10} cm^3 STP/g) are found in two unequilibrated samples (DaG 300 and 313), which contain a significant planetary gas component. Several other samples (DaG 328, 457, 458, and 757) also show $^{132}Xe/^{84}Kr$ ratios of ~1.0, but these are all based on very small amounts of trapped Kr and Xe (<10^{-10} cm^3 STP/g).

The amount of trapped atmospheric gases generally increases from weathering grade W1 to W4/W5, most notably for ^{84}Kr and ^{132}Xe. These observations indicate that the majority of the trapped heavy noble gases are atmospheric contamination carried by water into the meteorite during

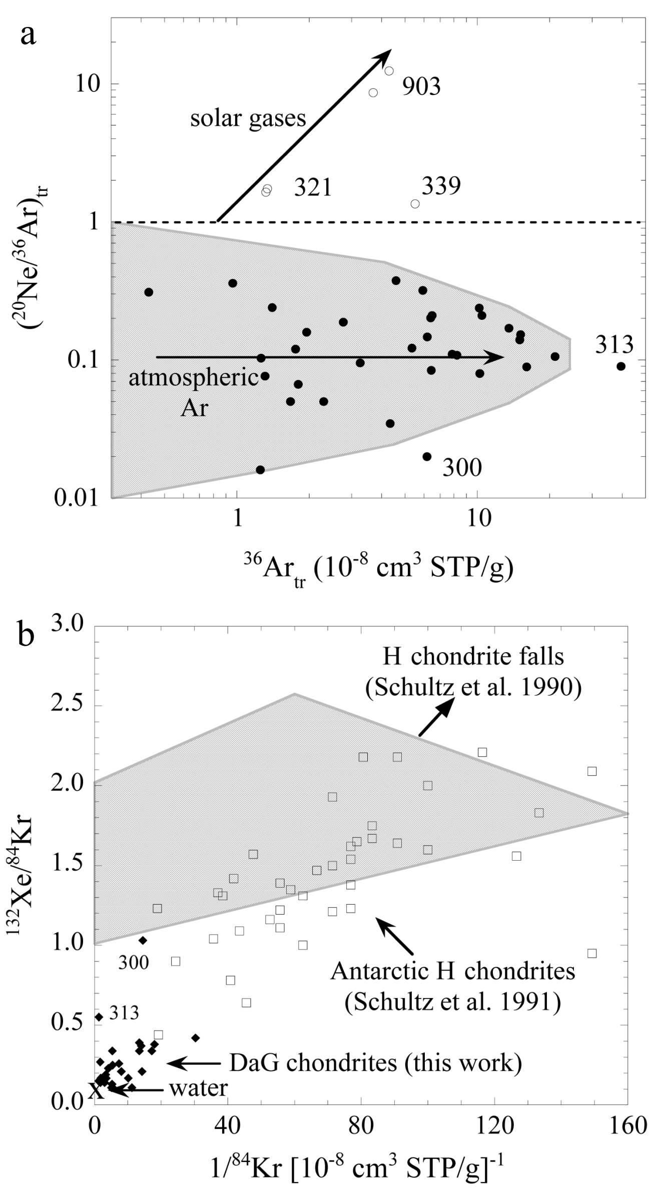

Fig. 2. Trapped noble gases in DaG samples. (a) shows that the trapped $^{20}Ne/^{36}Ar$ ratio in most DaG samples is <1 (closed circles), which indicates that trapped Ne and Ar in most of these samples are dominated by atmospheric contamination (grey area), while DaG 300 and 313 contain planetary gases. Only three samples (open circles) show a $^{20}Ne/^{36}Ar$ ratio >1, indicating a significant contribution of solar Ne. The high $^{20}Ne/^{36}Ar$ ratio in DaG 903 indicates a large solar gas component, while the $^{20}Ne/^{36}Ar$ ratios of 1.3–1.7 in DaG 321 and 339 indicate a small contribution of solar Ne. (b) shows the correlation of the $^{84}Kr/^{132}Xe$ ratio versus $1/^{84}Kr$ in DaG meteorites (solid symbols) compared to modern H chondrite falls (grey area; Schultz et al. 1990) as well as Antarctic H chondrites (open squares; Schultz et al. 1991). The low $^{84}Kr/^{132}Xe$ ratios of 0.1–0.4 in most DaG meteorites are much closer to the value of dissolved gases in water (represented by X) than to planetary values of 1.0–2.5, indicating trapped Kr and Xe are mainly due to atmospheric contamination brought into the samples via water. The higher $^{84}Kr/^{132}Xe$ ratios in DaG 300 and 313 indicate these unequilibrated meteorites contain a significant contribution of planetary Kr and Xe.

weathering (Scherer et al. 1994). However, based on the amount of trapped Ar, Kr, and Xe, DaG 304 (W4) and DaG 330 (W3) seem to be as much weathered as samples with weathering degree W5. Another interesting observation is that the amount of trapped ^{36}Ar varies by a factor of 2–7 between different aliquots of DaG 062, 304, and 311, as was also observed for other hot desert meteorites (Scherer et al. 1994; Stelzner et al. 1999). However, contrary to the results for six meteorites from the Acfer region in Algeria (Stelzner et al. 1999), we did not find any correlation between the amount of trapped Ar, Kr, and Xe and the terrestrial age of DaG meteorites (Table 3). This lack of correlation with terrestrial age suggests that the majority of the atmospheric noble gases is trapped within the first few thousand years after their fall, which is consistent with a scenario of rapid initial weathering proposed by Bland et al. (1998).

A correlation between measured ^{40}Ar and the estimated amount of trapped ^{36}Ar (=measured – cosmogenic) for DaG samples with high ^{40}Ar ($>5.5 \times 10^{-5}$ cm^3 STP/g) yields a slope of ~250 and an intercept of $^{40}Ar = 5.2 \times 10^{-5}$ cm^3 STP/g for $^{36}Ar_{tr} = 0$. The slope corresponds to an effective $^{40}Ar/^{36}Ar$ ratio of 250 for trapped Ar, while the intercept corresponds to a K-Ar age of 4.2–4.3 Gyr. This $^{40}Ar/^{36}Ar$ ratio of ~250 is lower than the atmospheric ratio of 296 but identical to the ratio found for trapped Ar in 15 fragments of the Gold Basin shower, an L4 chondrite with low radiogenic ^{40}Ar and with variable amounts of trapped Ar due to its 15 kyr residence in the desert of northwest Arizona (Kring et al. 2001; Welten et al. 2003). Since the concentration of atmospheric ^{36}Ar is correlated to the degree of weathering, the low $^{40}Ar/^{36}Ar$ ratio of the trapped Ar component is most likely an artifact of terrestrial weathering. Complete oxidation of the metal in H chondrites dilutes the concentration of radiogenic ^{40}Ar per gram sample by ~10%, thereby reducing the slope in the correlation of total ^{40}Ar versus trapped ^{36}Ar by 10–20% (assuming an atmospheric ^{36}Ar contribution of $1–2 \times 10^{-7}$ cm^3 STP/g). In addition, it cannot be excluded that the most weathered samples have lost a small amount of radiogenic ^{40}Ar.

Effect of Weathering on Cosmogenic and Radiogenic Noble Gases

Terrestrial weathering does not only lead to contamination with atmospheric noble gases but also results in lower concentrations of cosmogenic and radiogenic noble gases (Herzog and Cressy 1976; Gibson and Bogard 1978; Scherer et al. 1994). However, a recent study of Stelzner et al. (1999) on meteorites from the Acfer region in Algeria shows no evidence of radiogenic or cosmogenic noble gas losses in samples of weathering grade W4 and W5. For the DaG samples, we find no systematic decrease in the concentration of radiogenic ^{4}He as a function of the degree of weathering (as indicated by the Wlotzka scale). However, if we exclude the samples with low radiogenic ^{40}Ar ($<4 \times 10^{-5}$ cm^3 STP/g), we do find a trend of lower ^{4}He concentrations with increasing concentrations of trapped atmospheric ^{36}Ar (which provides an independent measure of the degree of weathering). From the observed trend, we estimate that a trapped atmospheric ^{36}Ar concentration of 10^{-7} cm^3 STP/g corresponds to a ~20% loss of radiogenic ^{4}He. This estimate implies that the most contaminated samples (DaG 304 and 330) may have lost up to ~40% of their radiogenic ^{4}He due to terrestrial weathering, while most samples have lost <20% of their radiogenic ^{4}He.

Based on elemental production rates, we estimate that ~20% of the $^{3}He_c$, ~1% of the $^{21}Ne_c$, and ~30% of the $^{38}Ar_c$ in H chondrites are produced in the metal fraction. This implies that oxidation of the metal may lead to significant losses of cosmogenic ^{3}He and ^{38}Ar, especially for H chondrites, while loss of ^{21}Ne should be negligible. Meteorites that have lost ^{3}He are easily identified since they show low $^{3}He/^{21}Ne$ ratios, while loss of cosmogenic Ar from weathered samples is less obvious due to the large amount of trapped atmospheric Ar. Figure 3 shows that the $^{3}He/^{21}Ne$ ratios in 27 of the 32 DaG samples (including samples of weathering category W4–W5) are within 20% of the $^{3}He/^{21}Ne$ versus $^{22}Ne/^{21}Ne$ correlation known as the Bern-line (Eberhardt et al. 1966). All of the five samples with low $^{3}He/^{21}Ne$ ratios (DaG 308, 321, 339, 904, and 908) show only minor to moderate degrees of weathering (W1–W3), which suggests that these samples did not lose large amounts of ^{3}He due to weathering. The most contaminated aliquots of DaG 304 (W4) show 10–15% lower $^{3}He/^{21}Ne$ ratios, indicating significant loss of cosmogenic ^{3}He. In contrast, the most weathered aliquot of DaG 062 (i.e., the sample with the highest amount of trapped Ar) shows no evidence of ^{3}He loss, which is consistent with the lower amount of metal in LL chondrites. These observations confirm that oxidation of the metal results in loss of cosmogenic ^{3}He (and ^{38}Ar), but the effects of ^{3}He loss are generally <20% for H chondrites and <10% for L and LL chondrites.

Since we conclude that the low $^{3}He/^{21}Ne$ ratios in five DaG samples are not due to weathering, this leaves the following possible explanations: i) very high shielding conditions (Masarik et al. 2001); ii) loss of ^{3}He and ^{4}He during ejection of the meteoroid from its parent body, as was observed for the Jilin H5 chondrite (Begemann et al. 1985); or iii) loss of ^{3}He due to solar heating in space (Hintenberger et al. 1966). The low $^{22}Ne/^{21}Ne$ ratios in DaG 308 and 904 indicate high shielding conditions, but the cosmogenic ^{10}Be and ^{26}Al concentrations are not as low as in Gold Basin, so very high shielding conditions do not seem to be a plausible explanation for the low $^{3}He/^{21}Ne$ ratios in any of the DaG samples. The other two explanations will be discussed in relation to the radiogenic ^{4}He and ^{40}Ar ages.

Cosmic Ray Exposure (CRE) Ages

The ^{21}Ne exposure ages show typical values for ordinary chondrites in the range of ~1 Myr to over 50 Myr (Fig. 4).

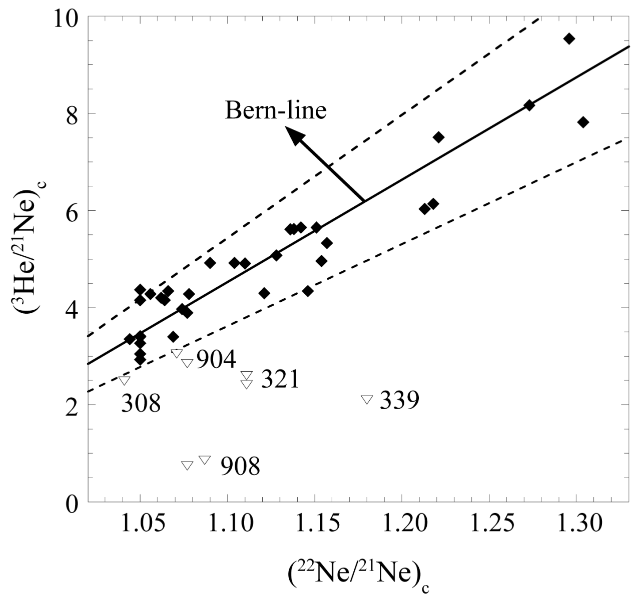

Fig. 3. Correlation of $(^{3}He/^{21}Ne)^c$ versus $(^{22}Ne/^{21}Ne)_c$ for all DaG samples listed in Table 1. The solid line represents the Bern-line, as defined by Nishiizumi et al. (1980), while the dashed lines represent variations from the Bern-line of ±20%. The closed symbols represent samples with no significant loss of cosmogenic ^{3}He, while the open symbols represent samples that seem to have lost more than 20% of their ^{3}He.

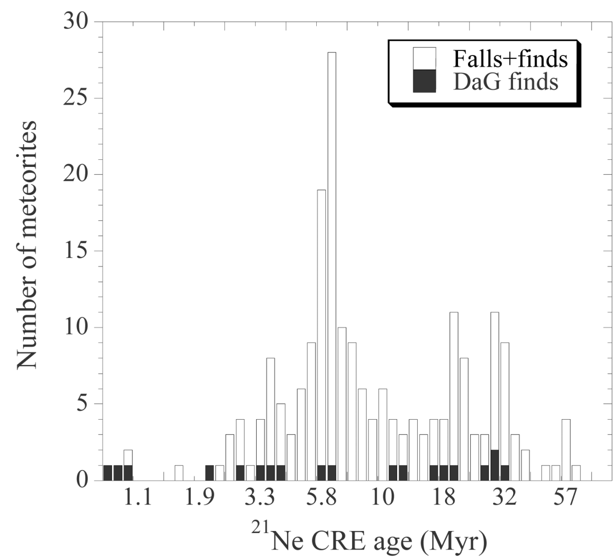

Fig. 4. Histogram of ^{21}Ne CRE ages of 19 H chondrites from the DaG region compared to those of 190 falls and finds (Graf and Marti 1995). The DaG H chondrites show few ages coinciding with the main H chondrite peak at ~7 Myr, while a relatively large fraction show ages <5 Myr.

Four of the H chondrite exposure ages coincide with the H chondrite peak at 33 Myr, while only two coincide with the main peak at ~7 Myr. Another unusual feature in the DaG age distribution is that eight of the 19 H chondrites (=42%) show exposure ages <5 Myr, while only 10–15% of modern H chondrite falls show exposure ages <5 Myr (Graf and Marti 1995). Interestingly, six out of those eight meteorites experienced high shielding conditions, as judged from their low $^{22}Ne/^{21}Ne$ ratios. Therefore, it is likely that, in our suite of DaG samples, the number of independent H chondrite falls with a CRE age <5 Myr is less than eight, because: i) possible pairings could reduce the six meteorites to three independent falls; and ii) for some of the meteorites with high shielding, the CRE age is probably underestimated. The latter follows from recent model calculations for large objects, which show that, at high shielding conditions, the simple relationship between the ^{21}Ne production rate and the $^{22}Ne/^{21}Ne$ ratio is not valid, resulting in an overestimation of the production rate (e.g., Graf et al. 1990; Leya et al. 2000; Masarik et al. 2001). To obtain more reliable ages for these samples, we also calculate CRE ages based on the $^{26}Al/^{21}Ne$ method (Graf et al. 1990) as discussed below.

Gas Retention Ages and their Relation to ^{3}He and ^{21}Ne Exposure Ages

The concentrations of radiogenic ^{4}He and ^{40}Ar correspond to U,Th-He ages of 0.1–4.3 Gyr and K-Ar ages of 0.5–4.5 Gyr, respectively. Only ~10% of the U,Th-He ages are >3.8 Gyr if we don't correct for the loss of radiogenic ^{4}He due to weathering. This number increases to ~30% if we do correct for weathering effects on the basis of the amount of atmospheric ^{36}Ar. In contrast, about 65% of the K-Ar ages are >3.8 Gyr, and the U,Th-He ages are always lower than the corresponding K-Ar ages (Fig. 6). These observations can be explained by the fact that ^{4}He is more easily lost from its host minerals than ^{40}Ar (Huneke et al. 1969). Another trend that follows from Fig. 5 is that the gas retention ages show a negative correlation with shock stage: samples with a low shock stage (S1–S2) show consistently high K-Ar ages of >3.8 Gyr, while lower K-Ar ages are only found in samples with shock stage S3–S6 (Fig. 5). This trend is consistent with previous observations (Stöffler et al. 1991; Schultz and Stöffler 1993). We find that low U,Th-He ages (<2.0 Gyr) and low K-Ar ages (<3.8 Gyr) are equally common among DaG H chondrites (5/19 = 26%) and L chondrites (2/7 = 28%), while low radiogenic ages are usually more common among L chondrites (Wasson and Wang 1991; Bogard 1995).

Figure 6 shows a plot of the ^{3}He-exposure-age/^{21}Ne-exposure-age ratio versus the radiogenic U,Th-He age/K-Ar age, or T_3/T_{21} versus T_4/T_{40}. This plot can be used to determine if radiogenic ^{4}He was lost before or after the start of cosmic ray exposure (Eugster et al. 1993). Figure 6 shows that most of the L chondrites (and one H chondrite, DaG 312) with low T_4/T_{40} ratios show T_3/T_{21} ratios between 0.8–1.2, which implies that they lost radiogenic ^{4}He and ^{40}Ar before they were exposed to cosmic rays, most likely due to large impacts on their parent body. However, the correlation of T_4/T_{40} versus T_3/T_{21} in most

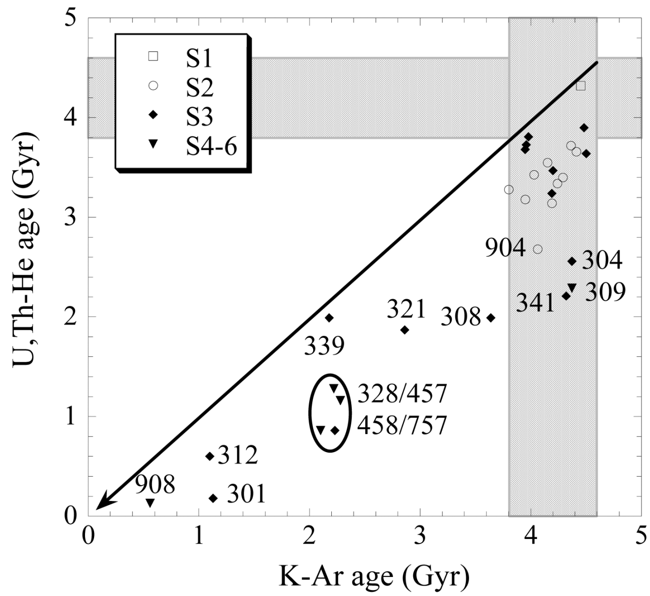

Fig. 5. Correlation of radiogenic U,Th-He and K-Ar ages. Samples with shock stage S1–S2 show high K-Ar ages (>3.8 Gyr), while all DaG samples with K-Ar ages <3.8 Gyr and U,Th-He ages <2.0 Gyr are more heavily shocked (S3–S6). Note also that the U,Th-He age is always lower than the K-Ar age.

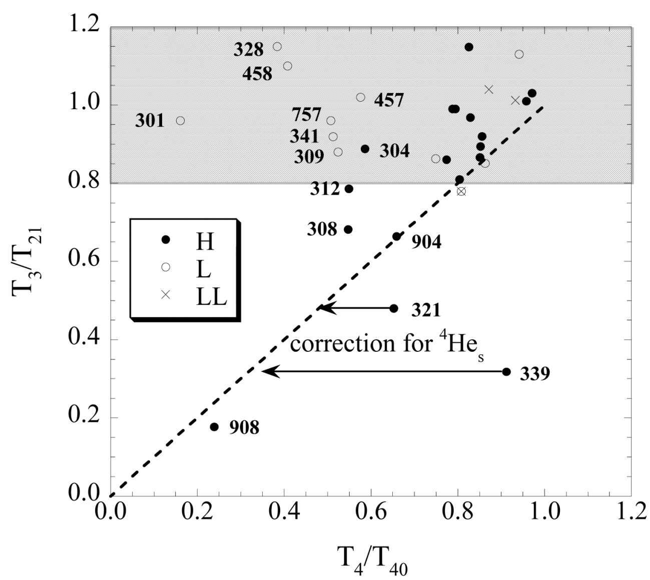

Fig. 6. Correlation of the cosmic ray exposure age ratio, T_3/T_{21}, versus the gas retention age ratio, T_4/T_{40}. Many L chondrites (open symbols) have lost radiogenic ^{4}He and ^{40}Ar before they were exposed to cosmic rays, while most H chondrites (closed symbols) with low radiogenic ages also show loss of cosmogenic ^{3}He, indicating that radiogenic ^{4}He was lost during cosmic ray exposure, either due to impacts on a precursor body or due to solar heating caused by orbits close to the sun. In addition, two samples with low T_4/T_{40} ratios (DaG 304 and 341) have probably lost ^{4}He due to weathering. The relatively high T_4/T_{40} ratios in DaG 339 (and to a lesser extent DaG 321) are due to a significant contribution of solar ^{4}He; corrections for solar He brings these samples closer to the 1:1 correlation.

DaG H chondrites with low T_4/T_{40} ratios (308, 321, 904, and 908) suggest that they lost both ^{4}He and ^{3}He after the onset of cosmic ray exposure. In contrast to previous studies, where none of the samples plot below the 1:1 correlation in a T_3/T_{21} versus T_4/T_{40} diagram (Eugster et al. 1993; Scherer et al. 1998), DaG 339 and (to a lesser extent) DaG 321 seem to be outliers with $T_3/T_{21} < T_4/T_{40}$ (Fig. 6). Since these two meteorites contain small—but detectable—amounts of solar Ne, we conclude that deviations from the 1:1 correlation are probably due to small contributions of solar ^{4}He, for which we did not correct. Thus, we estimate that DaG 321 and 339 contain ~150–390 × 10^{-8} cm^3 STP/g ^{4}He of solar origin, respectively. DaG 304 also shows a low T_4/T_{40} ratio, but its high K-Ar age (~4.4 Gyr) and high concentration of atmospheric Ar suggest that most of the ^{4}He loss is due to terrestrial weathering.

A question that we have not yet addressed is whether losses of radiogenic ^{4}He and cosmogenic ^{3}He in H chondrites are due to impacts on the parent/precursor body (Eugster et al. 1993) or to solar heating (Hintenberger et al. 1966; Schultz and Stöffler 1993). The first scenario requires a previous CRE on a larger body, while the second scenario requires an orbit with a perihelion close to the Sun. Our cosmogenic radionuclide results indicate that DaG 908 had a complex exposure history, so it is possible that, for this meteorite, most of the cosmogenic ^{3}He produced in the first stage and >95% of the radiogenic ^{4}He and ^{40}Ar were lost simultaneously during a recent breakup event. However, for the other four H chondrites with low T_3/T_{21} and low T_4/T_{40} ratios, we have no compelling evidence for a complex exposure history, so it seems likely that most of the gas losses in these meteorites are due to solar heating.

RADIONUCLIDES: TERRESTRIAL AGES AND PRE-ATMOSPHERIC SIZE

^{14}C and ^{14}C-^{10}Be Terrestrial Ages

The ^{14}C concentrations range from 1–35 dpm/kg. Based on average production rates of 46.4 dpm/kg for H, 51.1 dpm/kg for L, and 55.2 dpm/kg for LL chondrites, these concentrations correspond to terrestrial ages of 2.5–31.0 kyr, similar to ^{14}C ages of many other Saharan meteorites (Jull et al. 1990; Bland et al. 1998). For DaG meteorites in which ^{10}Be is saturated, based on the noble gas exposure age (Table 3), we calculated a shielding-corrected terrestrial age using the ^{14}C-^{10}Be method, assuming a ^{14}C/^{10}Be production ratio of 2.65 ± 0.15 (Jull et al. 2000). The thus derived ^{14}C-^{10}Be ages (Table 3) are in good agreement with the ^{14}C ages. Although the terrestrial ages do not show a clear correlation with the degree of weathering, the four oldest meteorites are also the most weathered (W3–W5), while meteorites younger than 10 kyr generally show only minor to moderate oxidation of the metal (W1–W3).

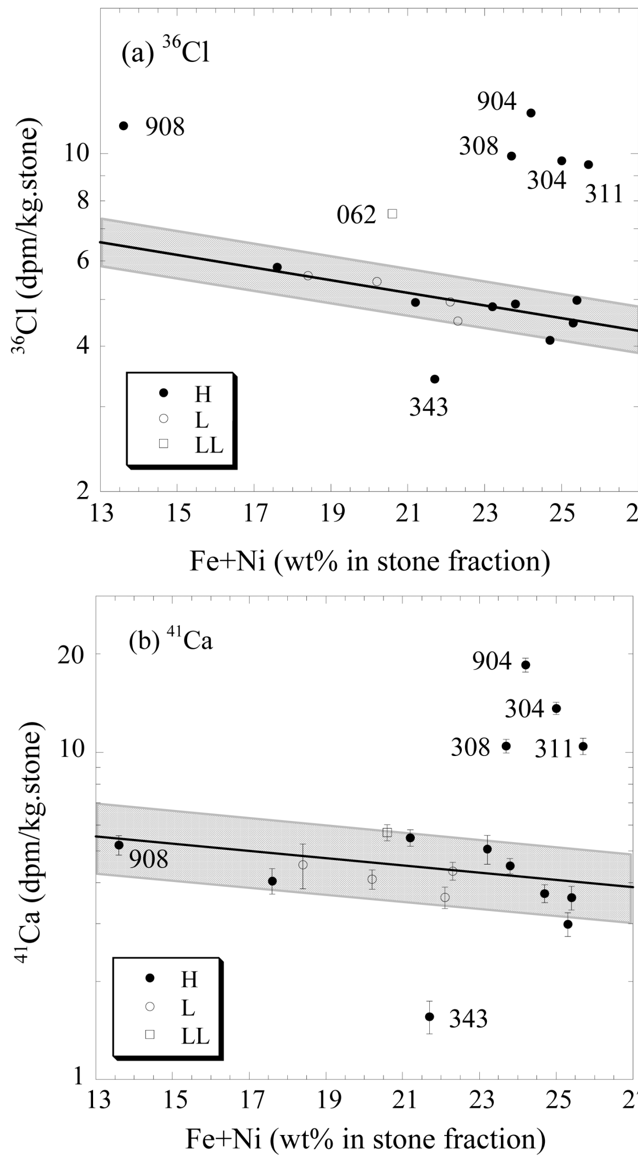

Fig. 7. Correlation of cosmogenic ^{36}Cl (a) and ^{41}Ca (b) versus total Fe + Ni in the stone fraction of 18 DaG samples. The negative correlation for about two-thirds of the samples indicates that cosmogenic ^{36}Cl and ^{41}Ca are lost from the oxidized metal phase during weathering. The addition of oxidized metal to the "stone" fraction increases concentrations of Fe and Ni, while it dilutes the concentrations of cosmogenic ^{36}Cl and ^{41}Ca. Elevated concentrations of ^{36}Cl and ^{41}Ca in four samples (DaG 304, 308, 311, 904) and of ^{36}Cl in one sample (DaG 908) are due to neutron-capture contributions, while the relatively low concentrations of ^{36}Cl and ^{41}Ca in DaG 343 indicate a terrestrial age >100 kyr.

^{36}Cl and ^{41}Ca Terrestrial Ages

The ^{36}Cl concentrations in the stone fraction range from 3–12 dpm/kg, although most (12) samples show values between 3–6 dpm/kg. The ^{36}Cl concentrations in 11 of these 12 samples show a negative correlation with the total Fe + Ni concentration (Fig. 7a), which increases with the amount of oxidized metal in the stone fraction (Welten 1999). This trend suggests that most of the cosmogenic ^{36}Cl produced in the metal phase is lost during weathering (oxidation) of the metal fraction. During magnetic separation of the metal, most of the ^{36}Cl-free oxidized metal ends up in the non-magnetic "stone" fraction, thereby diluting the cosmogenic ^{36}Cl concentration in the stone fraction. We assume that cosmogenic ^{36}Cl from troilite (FeS) is also lost during weathering, although our results do not provide clear evidence for or against this assumption. On the other hand, ^{36}Cl in clean metal should be retained, but for the more weathered meteorites, little or no clean metal could be separated.

Due to the loss of cosmogenic ^{36}Cl from metal and troilite during weathering, the measured ^{36}Cl concentrations should not be normalized to the measured concentration of Fe in the stone samples because part of this Fe is from oxidized metal and troilite. From chemical analyses of H chondrite falls (Jarosewich 1990), it follows that the non-metallic fraction contains 13.5 wt% Fe, of which ~9.5 wt% is in silicates and ~4.0 wt% in troilite. We normalized the measured ^{36}Cl concentration in H chondrite samples to a Fe concentration of 13.5 wt% for samples with minor weathering (W1), decreasing to a Fe concentration of 9.5% for the most weathered samples (W4/5). The latter value is based on the assumption that, in the most weathered samples, all troilite is oxidized, while only the ^{36}Cl produced from Fe in silicate minerals is retained. Based on chemical analyses of Jarosewich (1990), similar normalizations were done for L and LL chondrites, assuming Fe concentrations decreasing from 16–17 wt% for fresh L and LL's (W1) to 12–13 wt% for weathered L and LL's (W4/5). We accounted for the production of ^{36}Cl from Ca and K by adopting production rate ratios of $P(^{36}Cl)_{Ca}/P(^{36}Cl)_{Fe} = 8$ (Begemann et al. 1976) and $P(^{36}Cl)_K/P(^{36}Cl)_{Ca} = 1.8$ (Welten et al. 2000).

The ^{41}Ca concentrations in the stone fraction range from 1.6–18.5 dpm/kg, although most samples (13) show values between 3–6 dpm/kg. The concentrations of ^{41}Ca in these samples show a similar correlation with total Fe + Ni (Fig. 7b) as those of ^{36}Cl, indicating that cosmogenic ^{41}Ca in the metal phase is also lost upon oxidation. Therefore, we normalized the ^{41}Ca concentrations in the same way as the ^{36}Cl concentrations, assuming a production rate ratio of ^{41}Ca from Ca relative to that from Fe, $P(^{41}Ca)_{Ca}/P(^{41}Ca)_{Fe} = 6$ (Vogt et al. 1991). In addition, we corrected for the dilution with oxidized metal, which is up to 15% for H chondrites but <10% and <5% for L and LL chondrites, respectively (Welten 1999).

The normalized and dilution-corrected ^{36}Cl concentrations (Fig. 8a) show values of 20–26 dpm/kg(Fe + 8Ca + 15K) for most samples, which is consistent with the ^{14}C terrestrial ages <30 kyr. The normalized ^{36}Cl concentration of ~16 dpm/kg for DaG 343 corresponds to a terrestrial age of ~150 kyr but has a large uncertainty. The high ^{36}Cl concentrations of 40–56 dpm/kg(Fe + 8Ca + 15K) in DaG 304, 308, 311, 904, and 908 are due to neutron-capture ^{36}Cl,

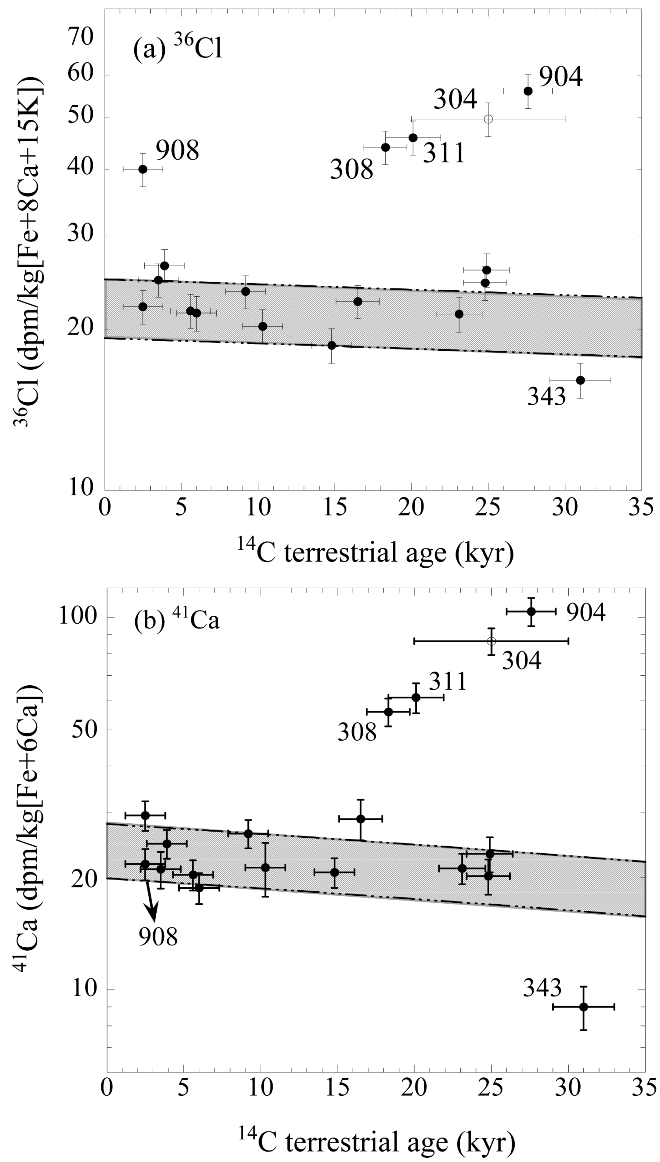

Fig. 8. Correlation of cosmogenic ^{36}Cl (a) and ^{41}Ca (b) in the stone fraction (normalized to the amount of Fe + xCa + yK) versus the ^{14}C-derived terrestrial age (closed symbols). In the absence of ^{14}C data for DaG 304, its terrestrial age was estimated at 25 ± 5 kyr from the degree of weathering (open symbol). If we exclude the samples (DaG 304, 308, 311, 904, and 908) with large contributions of neutron-capture products, the ^{36}Cl and ^{41}Ca concentrations in most samples are consistent with terrestrial ages <30 kyr. The only exception is DaG 343, for which the ^{14}C concentration of ~1 dpm/kg only gives a lower limit of ~30 kyr, while the ^{41}Ca concentration of ~9 dpm/kg(Fe + 6Ca) corresponds to a terrestrial age of 150 ± 40 kyr, which is also in agreement with the age of 100–200 kyr derived from ^{36}Cl.

indicating a large pre-atmospheric size of these meteorites. For meteorites with large contributions of neutron-capture products, the ^{36}Cl and ^{41}Ca concentrations in the stone fraction can obviously not be used to calculate terrestrial ages.

The normalized ^{41}Ca concentrations show a slight decrease with the ^{14}C terrestrial age (Fig. 8b), but the uncertainties in the ^{41}Ca values are too large to determine terrestrial ages on a timescale of <30 kyr. However, the normalized ^{41}Ca concentration of ~8 dpm/kg for DaG 343 corresponds to a terrestrial age of 150 ± 40 kyr. This age is consistent with the ^{36}Cl terrestrial age but is much longer than the ^{14}C age of 31 kyr. The ^{14}C age of DaG 343, therefore, should only be considered as a lower limit because contamination with terrestrial CO_2 may be a problem at the level of ~1 dpm ^{14}C/kg. With a terrestrial age of ~150 kyr, DaG 343 is the oldest chondrite found outside Antarctica, with exception of the 480 Myr old "fossil chondrites" found embedded in Ordovician limestone in Sweden (Schmitz et al. 2001).

The long terrestrial age for DaG 343 indicates that not only achondrites but also ordinary chondrites can survive longer than 50 kyr in hot deserts. Schlüter et al. (2002) suggested that meteorites may have been protected from wet periods in the Sahara, such as the one between 11,000 and 3000 years ago, by soil coverage. This soil was removed by deflation during the current arid period, exhuming the meteorites. Fig. 9 shows that the terrestrial age distribution of chondrites at DaG is similar to the age distribution of those found in Acfer (Algeria), while those found in the Daraj region (Western Libya) tend to be younger. The younger terrestrial ages at Daraj may be explained by the somewhat wetter conditions in this area, resulting in faster weathering rates than in the DaG region (Abu Aghreb et al. 2003).

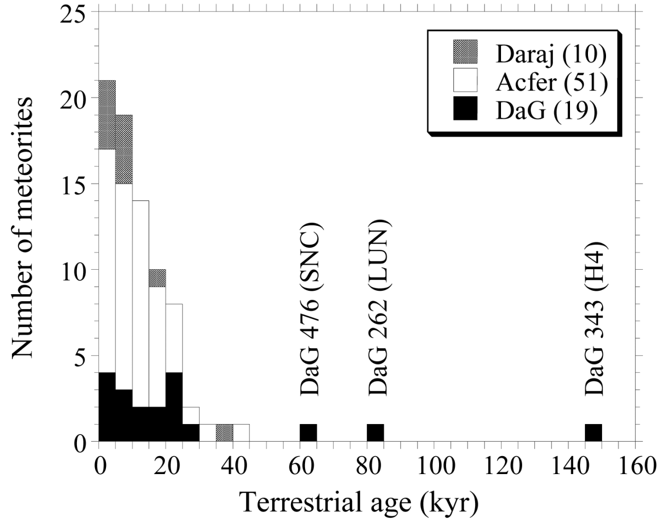

Fig. 9. Histogram of terrestrial ages of Saharan meteorites. The histogram includes 17 DaG chondrites studied in this work, 10 chondrites from the Daraj region in western Libya (Jull et al. 1990), and 51 chondrites from the Acfer region in Algeria (Bland et al. 1998), as well as two DaG achondrites (Nishiizumi et al. 1998; 2001).

Pre-Atmospheric Size and Exposure History

The ^{10}Be and ^{26}Al concentrations range from 5–21 and 25–54 dpm/kg, respectively. Considering the terrestrial ages of <30 kyr for most samples, the variations in ^{10}Be and ^{26}Al must be due to differences in shielding effects and exposure history. Three samples (DaG 304, 904, and 908) show low ^{10}Be concentrations (5.1–7.7 dpm/kg) and high $^{26}Al/^{10}Be$ ratios (4.8–5.2), which indicate short exposure ages. If we assume a maximum $^{26}Al/^{10}Be$ production rate ratio of 3.5, then the measured ratios correspond to exposure ages of less than 1.5–2.0 Myr, consistent with their ^{21}Ne exposure ages of 0.8–1.0 Myr.

The high ^{41}Ca values of 55–104 dpm/kg(Fe + 6Ca) in four samples (DaG 304, 308, 311, and 904) are clearly due to neutron-capture produced ^{41}Ca. These values correspond to specific ^{41}Ca activities (at saturation) of 0.4–0.5 dpm/gCa for DaG 308 and 311 up to values of 0.9–1.1 dpm/kg for DaG 304 and 904, respectively. The large contributions of neutron-capture ^{36}Cl and ^{41}Ca indicate that these four meteorites had large pre-atmospheric radii (R >50 cm), which is consistent with their low $^{22}Ne/^{21}Ne$ ratios.

Exposure History of DaG 908

The low concentrations of ^{10}Be and ^{26}Al in the stone fraction of DaG 908 are consistent with a simple CRE history of 0.8–1.0 Myr, while the high neutron-capture-produced ^{36}Cl indicates high shielding. The only result inconsistent with this simple exposure history is the low concentration of ^{41}Ca, which indicates a low thermal-neutron flux and, thus, a small pre-atmospheric size (R <30 cm). This can only be explained by a recent breakup event, which must have occurred 0.2–0.4 Myr ago, i.e., long enough for a significant part (i.e., >75%) of the neutron-capture ^{41}Ca (produced in the first stage) to decay but short enough to retain ~40–60% of the neutron-capture-produced ^{36}Cl. The measured ^{41}Ca concentration of 18.9 ± 0.9 dpm/kg in the metal phase is significantly lower than expected for small meteorites (24 ± 2 dpm/kg), which suggests that the recent irradiation in a small object could not have been longer than ~0.2 Myr. Based on a measured $^{26}Al/^{10}Be$ ratio of 5.2 in the stone fraction and a recent irradiation of ~0.2 Myr, we constrain the first-stage exposure to ~0.8 Myr. The ^{10}Be concentrations of 1.34 ± 0.05 dpm/kg in the metal and 7.7 ± 0.1 dpm/kg in the stone fraction indicate production rates of 2.7–3.3 dpm/kg in the metal and 19–23 dpm/kg in the stone during the first-stage irradiation. These production rates suggest a radius of 70–110 cm (Welten et al. 2001).

The ^{26}Al concentration of 2.07 ± 0.05 dpm/kg in the metal also reflects a short irradiation at high shielding, but the $^{26}Al/^{10}Be$ ratio of 1.54 ± 0.07 in the metal is ~25–30% higher than the expected ratio for the proposed exposure scenario. Assuming a $P(^{26}Al)/P(^{10}Be)$ ratio of 0.68–0.72 (Albrecht et al. 2000), this high $^{26}Al/^{10}Be$ ratio cannot be explained by any other exposure scenario but must be due to significant phosphorus (and possibly sulphur) in the metal fraction. Calculations by Leya and Michel (1998) show that, in the center of an object with a radius of ~350 g/cm^2 (corresponding to R ~1 m for chondrites), only 0.2–0.3% P + S is needed in the metal to increase $P(^{26}Al)$ by 25–30%.

We conclude that DaG 908 experienced two impact events in the last ~1 Myr: the first impact ~1 Myr ago ejected an object with a radius of 70–110 cm from its parent body, and the second impact ~0.2 Myr ago, resulted in a breakup of this object into smaller pieces, one of which (DaG 908) eventually collided with Earth. It is interesting to note that the ^{3}He exposure age of ~0.14 Myr agrees fairly well with the recent irradiation of ~0.2 Myr deduced from the radionuclide concentrations. This could indicate that >95% of the cosmogenic ^{3}He produced in the first stage as well as most of the radiogenic ^{4}He was lost during the recent breakup event. A similar scenario was also proposed for the Jilin H5 chondrite, which lost most of its cosmogenic ^{3}He produced in the first stage as well as most of its radiogenic ^{4}He during excavation from its parent body ~0.4 Myr ago (Begemann et al. 1985, 1996). However, since we have only one data point for DaG 908, the evidence for a short thermal event is not as strong as for Jilin, and, therefore, we cannot exclude that loss of He and radiogenic ^{40}Ar occurred more gradually due to solar heating in a low-perihelion orbit.

EXPOSURE AGES BASED ON ^{26}Al/^{21}Ne AND ^{10}Be/^{21}Ne RATIOS

Both model calculations and empirical studies have shown that the ^{21}Ne production rate is not simply a function of the ^{22}Ne/^{21}Ne ratio but scatters widely for low ^{22}Ne/^{21}Ne ratios. The semi-empirical model of Graf et al. (1990) suggests that the ^{10}Be/^{21}Ne and ^{26}Al/^{21}Ne ratios are relatively insensitive to shielding and, thus, provide an alternative method for calculating exposure ages for high shielding. However, recent model calculations (Leya et al. 2000) suggest that the P(^{10}Be)/P(^{21}Ne) ratio is much more dependent on shielding than suggested by Graf et al. (1990). For high shielding conditions (^{22}Ne/^{21}Ne <1.10), the model by Leya et al. (2000) yields 20–40% lower P(^{10}Be)/P(^{21}Ne) ratios than the model of Graf et al. (1990). These large discrepancies between the two models make the ^{10}Be/^{21}Ne method less reliable. The ^{26}Al/^{21}Ne production rate ratio in chondrites is less dependent on shielding than the ^{10}Be/^{21}Ne ratio since the size and depth dependence of the ^{21}Ne production is more similar to that of ^{26}Al production than to ^{10}Be production. The model of Leya et al. (2000) yields P(^{26}Al)/P(^{21}Ne) ratios, which increase from 0.36–0.37 for L chondrites with radii between 25 and 120 cm to 0.40–0.42 for objects with a radius of 5 cm. In comparison, model calculations using the LAHET Code System yield only slightly higher ratios of 0.40–0.45 (Masarik and Reedy 1994). For our exposure age calculations, we used the following equation to determine the ^{26}Al/^{21}Ne production rate ratio as a function of the ^{22}Ne/^{21}Ne ratio in each sample:

$$P(^{26}Al)/P(^{21}Ne) = 0.375 + 0.20*(^{22}Ne/^{21}Ne - 1.11) \quad (1)$$

This equation yields P(^{26}Al)/P(^{21}Ne) ratios ranging from 0.36 atom/atom in the most shielded samples to a ratio of ~0.41 atom/atom in the least shielded samples, consistent with the model of Leya et al. (2000). Exposure ages are calculated from the measured concentrations of ^{21}Ne in bulk

Table 5. Cosmic ray exposure ages, T in Myr, based on ^{21}Ne concentrations in DaG meteorites. Exposure ages are either based on the correlation between P(^{21}Ne) and ^{22}Ne/^{21}Ne (Eugster 1988) or on a relatively constant production ratio of the ^{21}Ne/^{26}Al nuclide pair (Graf et al. 1990). Measured ^{21}Ne/^{26}Al ratios and production rate ratios, P(^{26}Al)/P(^{21}Ne), calculated using Equation 1, are given in atom/atom. Measured ^{21}Ne/^{10}Be ratios and ^{21}Ne/^{26}Al exposure ages are then used to estimate the ^{10}Be/^{21}Ne production rate ratios in these samples.

DaG	Type	^{22}Ne/^{21}Ne	P(^{26}Al)/P(^{21}Ne)	T(^{21}Ne)	^{21}Ne/^{26}Al	T(^{26}Al/^{21}Ne)	P(^{21}Ne)	^{21}Ne/^{10}Be	P(^{10}Be)/P(^{21}Ne)
304	H6	*1.05*	0.363	0.8	5.5	1.6	0.206	12.8	0.110
308	H6	1.041	0.361	2.6	13.5	5.0	0.234	20.7	0.124
311	H6	1.044	0.362	3.7	20.3	7.4	0.219	29.1	0.122
312	H6	1.121	0.377	31.6	123.4	45.1	0.207	146.7	0.149
321	H5	1.111	0.375	7.4	23.7	9.3	0.245	30.1	0.141
322	H4	1.221	0.397	19.6	49.5	21.6	0.188	64.7	0.144
336	H5/6	1.138	0.381	3.4	10.1	3.8	0.250	13.4	0.158
339	H5	*1.18*	0.389	6.6	17.3	6.8	0.226	23.3	0.141
343	H4	1.288	0.411	4.7	10.6	4.4	0.184	13.7	0.171
388	H5/6	1.077	0.368	31.5	118.3	44.3	0.258	152.0	0.135
904	H6	1.075	0.368	1.0	7.5	2.6	0.146	17.6	0.097
907	H6	1.090	0.371	13.6	48.8	18.4	0.251	57.4	0.148
908	H6	*1.08*	0.369	0.77	4.1	0.94	0.287	9.9	0.125
330	L5	1.154	0.384	9.1	26.2	10.2	0.247	35.1	0.136
341	L6	1.157	0.384	12.1	35.2	13.8	0.241	44.2	0.144
342	L5–6	1.069	0.367	41.9	166.6	62.1	0.275	208.5	0.138
906	L6	1.296	0.413	4.8	11.7	4.9	0.178	14.7	0.172
062	LL5–6	1.134	0.380	12.2	34.7	13.4	0.269	43.7	0.142

samples and of ^{26}Al in the stone fraction after the latter were corrected for radioactive decay during the terrestrial residence times of 0–150 kyr and normalized to bulk samples. The normalization of ^{26}Al to bulk was done by correcting for the estimated amount of unoxidized metal that we separated from bulk samples (Table 4), assuming that the metal has 10–20 times lower ^{26}Al than the stone fraction (Nagai et al. 1993). Using P(^{26}Al)/P(^{21}Ne) ratios from Table 5, the obtained ^{21}Ne/^{26}Al ratios in the bulk (b) were then converted to exposure ages, T (in Myr), according to the following equation:

$$T/(1 - e^{-\lambda T}) = (^{21}Ne/^{26}Al)_b * 1.017 * P(^{26}Al)/P(^{21}Ne) \quad (2)$$

where λ is the decay constant of ^{26}Al (in Myr^{-1}). The low ^{26}Al concentrations in DaG 304, 308, 311, and 904 lead to ^{26}Al/^{21}Ne ages that are 1.8–2.6 times higher than the corresponding ^{21}Ne ages (Fig. 10). These are also the four samples with large contributions of neutron-capture ^{36}Cl and ^{41}Ca, so the lower ^{21}Ne production rates that follow from the ^{26}Al/^{21}Ne method are consistent with their large pre-atmospheric size and confirm that the relation between P(^{21}Ne) and the ^{22}Ne/^{21}Ne ratio is not unambiguous.

The ^{26}Al/^{21}Ne age of ~1.6 Myr for DaG 304 is consistent with its high ^{26}Al/^{10}Be ratio of ~4.9. This short age yields ^{10}Be and ^{26}Al production rates of 11.7 and 37.5 dpm/kg, respectively, which are consistent with the high shielding conditions of DaG 304. The ^{26}Al/^{21}Ne ages for DaG 308 and 311 correspond to ^{10}Be production rates of 13.6 dpm/kg (DaG 311) and 15.2 dpm/kg (DaG 308). These production rates indicate somewhat lower shielding conditions than in DaG 304, which is consistent with the lower neutron-capture ^{36}Cl and ^{41}Ca concentrations in DaG 308/311. The ^{26}Al/^{21}Ne ages of DaG 304/308/311 correspond to ^{21}Ne production rates of 0.20–0.23 × 10^{-8} cm^3 STP/g.Myr, i.e., almost a factor of two lower than those predicted by the correlation of Eugster (1988). Interestingly, the revised CRE age of DaG 311 now coincides with the main H chondrite peak at ~7 Myr. The only inconsistency is found for DaG 904, for which the ^{26}Al/^{21}Ne age of 2.7 Myr is significantly higher than the maximum CRE age of 2.0 Myr, which we derived from the ^{26}Al/^{10}Be ratio. A recent exposure age of 2.7 Myr would imply an unrealistically high ^{26}Al/^{10}Be production rate ratio of ~3.8, which is higher than measured ratios of 3.3–3.5 in large chondrites, such as Chico (Garrison et al. 1992), Ghubara (Ferko et al. 2002), and Gold Basin (Welten et al. 2003). Thus, for DaG 904, we have to consider a complex exposure history with a first-stage exposure on the parent body followed by a 4π exposure of 1–2 Myr as a large object. The complex exposure histories of DaG 904 and 908 confirm the trend observed by Herzog et al. (1997) that many meteorites with "short" CRE ages have complex exposure histories.

Samples with ^{22}Ne/^{21}Ne ratios >1.13 show ^{26}Al/^{21}Ne ages that agree, within the experimental uncertainty of ~20%, with the ^{21}Ne ages. However, for five meteorites with ^{22}Ne/^{21}Ne ratios of 1.07–1.12, the ^{26}Al/^{21}Ne ages are 25–50% higher than the corresponding ^{21}Ne ages. The higher ^{26}Al/^{21}Ne ages are due to relatively low ^{26}Al concentrations of 38–52 dpm/kg, i.e., 20–40% lower than would be expected for medium-sized objects with ^{22}Ne/^{21}Ne ratios of 1.07–1.12. Low ^{26}Al production rates occur in very large objects (R >60 cm) as well as in very small objects (R <20 cm). Since the absence of neutron-capture ^{36}Cl and ^{41}Ca rules out a large pre-atmospheric size, we conclude that these meteorites were relatively small in the last few Myr of their exposure. In contrast, the low ^{22}Ne/^{21}Ne ratios indicate that their "average size" (during their entire exposure history) must have been significantly larger, i.e., these meteorites were previously exposed under higher shielding conditions, either on the surface of their parent body or in a larger object in space. Since the half-lives of the radionuclides used in this study are too short to constrain the exposure history of these samples, we will assume that the ^{21}Ne exposure ages for these samples are the most reliable.

Since the ^{26}Al/^{21}Ne exposure age method seems fairly robust (Leya et al. 2001), we can use the ^{26}Al/^{21}Ne ages of the DaG meteorites to determine the ^{10}Be/^{21}Ne production rate ratios from the measured ^{10}Be and ^{21}Ne concentrations in these samples. We exclude DaG 904 and 908 from this exercise since these samples show clear evidence of a complex exposure history. The resulting P(^{10}Be)/P(^{21}Ne)

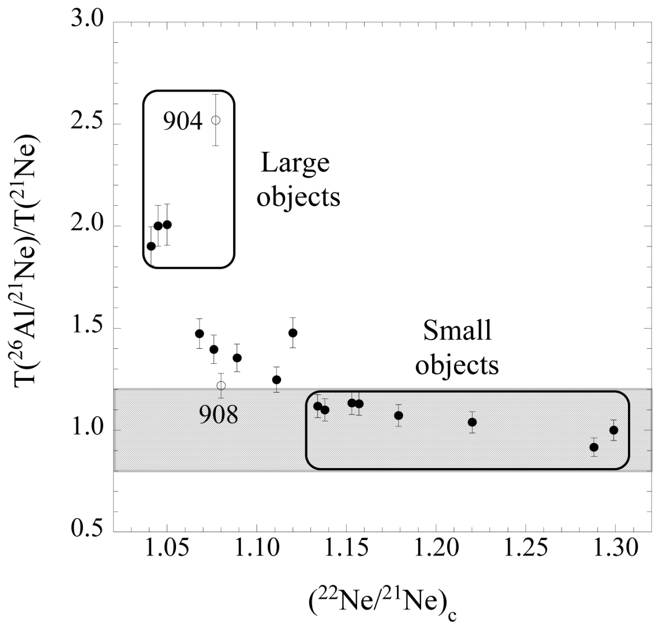

Fig. 10. Dependence of the T(^{26}Al/^{21}Ne)/T(^{21}Ne) exposure age ratio as a function of the ^{22}Ne/^{21}Ne ratio. For small objects (with ^{22}Ne/^{21}Ne ratios >1.13), the two ages show good agreement, while for large objects (with ^{22}Ne/^{21}Ne ratios <1.09 and significant contributions of neutron-capture ^{36}Cl and ^{41}Ca), the ^{26}Al/^{21}Ne age is 1.8–2.6 times higher than the ^{21}Ne age. These results confirm that the relation between the ^{21}Ne production rate and the ^{22}Ne/^{21}Ne ratio is not unambiguous.

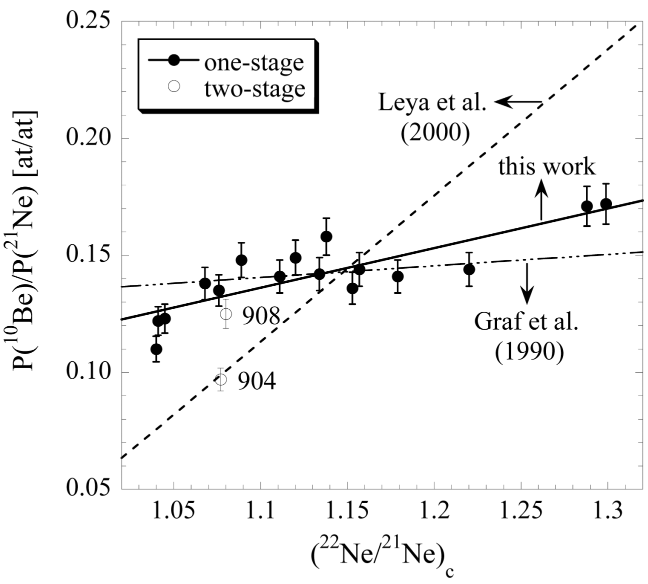

Fig. 11. The $^{10}Be/^{21}Ne$ production rate ratio as a function of the cosmogenic $^{22}Ne/^{21}Ne$ ratio. The production rate ratios are based on measured ^{10}Be, ^{26}Al, and ^{21}Ne concentrations in 18 DaG samples and $T(^{10}Be/^{21}Ne) = T(^{26}Al/^{21}Ne)$ and $P(^{26}Al)/P(^{21}Ne)$ is calculated using Equation 1. The solid line represents a linear fit through the solid symbols (this study), which represent samples with a simple exposure history. The dashed line represents the correlation derived by the physical model of Leya et al. (2000), the semi-dashed line the semi-empirical correlation of Graf et al. (1990).

ratios in the remaining 16 samples range from 0.11–0.17. Figure 11 shows that this range is significantly larger than the range of 0.138–0.150 predicted by Graf et al. (1990) but much smaller than the range of 0.08–0.21 proposed by Leya et al. (2000). We find a fairly good correlation (R = 0.84) of the $P(^{10}Be)/P(^{21}Ne)$ ratio with the $^{22}Ne/^{21}Ne$ ratio:

$$P(^{10}Be)/P(^{21}Ne) = 0.138 + 0.17*(^{22}Ne/^{21}Ne - 1.11) \quad (3)$$

We estimate that the uncertainties in the derived $P(^{10}Be)/P(^{21}Ne)$ ratios are 5–7% for objects with radii of 5–100 cm, while the ratios in very large objects, such as the Gold Basin meteoroid (R = 3–5 m; Welten et al. 2003), may be ~10% lower than predicted by Equation 3.

PAIRING AND SHOWERS

One of the fundamental pieces of information that we can obtain from the distribution and terrestrial ages of hot desert meteorites is the meteorite infall rate (to the Earth) over the past 10–50 kyr (Bland et al. 1996). To determine this flux, it is important to identify paired specimens and large strewnfields, as was first done for the DaG meteorites using classification characteristics and find location only (Schlüter et al. 2002). Here, we add the noble gas and radionuclide data to evaluate some of the pairings proposed by Schlüter et al. (2002) and to identify additional pairings.

The large pairing group of L6 chondrites DaG 328, 457, 458, and 757 is confirmed by the high CRE ages and low U,Th-He and K-Ar ages. DaG 757 has an ~30% lower ^{21}Ne exposure age than the other three L6 chondrites, but this may be due to different shielding conditions for which the low $^{22}Ne/^{21}Ne$ ratio (~1.07) does not correct properly. Unfortunately, no radionuclide data are available for these samples to verify this difference in shielding. Based on the CRE age alone, DaG 342 may also be part of this shower, but its radiogenic gases and different find location (78 km apart form the DaG 328 strewnfield) seem to rule out pairing. We can also rule out the proposed pairing of DaG 341/906 because they show very different CRE ages, radiogenic ages, and terrestrial ages. Since none of the other L or LL chondrites are paired, this reduces the 13 L and LL chondrites to 10 independent falls.

None of the selected H chondrites are paired specimens based on classification characteristics and find location alone (Schlüter et al. 2002). However, as we mentioned before, it is striking that a relatively large portion of the H chondrites (6 out of 19) show short exposure ages (<5 Myr) and high shielding conditions ($^{22}Ne/^{21}Ne$ <1.08), which suggests that some of these specimens may be paired. DaG 908 is clearly a distinct fall, based on its complex exposure history and very low radiogenic gas ages. Of the remaining five H chondrites with high shielding, we suggest two possible pairing groups based on the available noble gas and radionuclide data: i) DaG 304/904, and ii) DaG 308/311/905. The very similar radionuclide concentrations (low ^{10}Be and ^{26}Al combined with high ^{36}Cl and ^{41}Ca) in DaG 304/904 and the relatively short distance of 5.3 km between their locations of find support pairing. The 15% difference in the ^{21}Ne concentration and the 40% difference in $^{21}Ne/^{10}Be$ and $^{21}Ne/^{26}Al$ ratios could be used as an argument against pairing but can also be explained by a complex exposure history of a large object, in which DaG 904 acquired a small amount of ^{21}Ne on the parent body, while DaG 304 was buried deep enough to avoid significant production of ^{21}Ne. Of the second pairing group, DaG 311 and 905 form the most likely pair because of similar radiogenic ages and relatively close find locations (5.5 km apart), while DaG 308 was found ~26 km to the north. Other possible H chondrite pairings are DaG 300/322 and 302/388, although the find locations of the members of these two pairs are 17.5 and ~50 km apart, respectively. These possible pairings reduce the 19 H chondrites to a minimum of 14 different falls.

Whether they are paired or not, the large pre-atmospheric sizes of DaG 304, 308, 311, 904, and 905 suggest that these five H chondrites may be part of several large (unrecognized) showers. Maybe these showers went unnoticed because their strewnfields were more widely dispersed than those identified by Schlüter et al. (2002). An example of such a large strewnfield is the group of five shergottites (DaG 476/489/670/735/876) that were found up to 58 km apart. Our conclusion based on cosmogenic nuclide data supports the suggestion of Schlüter et al. (2002) that several unidentified H chondrite showers are present, which would explain the high H/L chondrite ratio of 1.6 at DaG compared to a ratio of 0.92 for ordinary chondrite falls (Grady 2000). It must be noted that high H/L chondrite ratios are also found in several Antarctic meteorite collections, such as those from the Allan Hills (Huss 1991), the Lewis Cliff (Cassidy et al. 1992), and the Frontier Mountain ice fields (Welten et al. 1999). In all these cases, the high ratio was attributed to one or several large H chondrite showers. Harvey (2003) recently pointed out that, among well-documented falls, H chondrites are 50% more likely to produce showers of more than 10 fragments than L chondrites. Although no physical reason was given for this observation, it may explain the trend of high H/L chondrite ratios at Antarctic and non-Antarctic collection sites.

CONCLUSIONS

The terrestrial ages of most DaG samples are <30 kyr, based on ^{14}C. The only exception is DaG 343 (H4), which has a terrestrial age of 150 ± 40 kyr, based on ^{36}Cl and ^{41}Ca concentrations. DaG 343 is the oldest ordinary chondrite found in any desert outside Antarctica, indicating that not only achondrites can survive the hot desert environment for more than 50 kyr, but ordinary chondrites can as well.

Noble gases and cosmogenic radionuclide concentrations indicate that the 32 DaG meteorites studied represent between 25 and 29 individual falls. Four H chondrites show significant contributions of neutron-capture ^{36}Cl and ^{41}Ca, indicating a large pre-atmospheric size (R >50 cm), which suggests that they may be part of several large unrecognized showers. The presence of these showers could help to explain the high H/L chondrite ratio in the DaG meteorite collection relative to ordinary chondrite falls.

The trapped noble gases are dominated by atmospheric gases, which increase with the degree of weathering, especially for ^{84}Kr and ^{132}Xe. The amount of atmospheric contamination is not related to terrestrial age, which suggests that the majority of atmospheric noble gases are trapped within the first few hundred years after their fall. In addition to atmospheric gases, we identified planetary gases in two unequilibrated chondrites (DaG 300 and 313) and solar gases in three chondrites (DaG 321, 339, and 903).

Gas retention ages based on U,Th-He range from 0.1–4.4 Gyr, while most K-Ar ages are between 3.8–4.5 Gyr. Ten DaG samples show significant losses of radiogenic ^{40}Ar, corresponding to ages of <3.6 Gyr. The difference between H and L chondrites with low radiogenic ages is interesting: the L chondrites lost radiogenic gases before cosmic ray exposure due to impacts on the parent body, while the H chondrites lost radiogenic gases (as well as cosmogenic ^{3}He) during cosmic ray exposure, either due to impacts on the parent body or to solar heating. In addition, some of the most weathered samples show significant losses of radiogenic ^{4}He (and cosmogenic ^{3}He) due to terrestrial weathering, while the K-Ar ages seem little affected by weathering.

We calculated CRE ages using the correlation of ^{21}Ne versus ^{22}Ne/^{21}Ne for small meteorites and the ^{26}Al/^{21}Ne method for meteorites with a large pre-atmospheric size. CRE ages of L chondrites are dominated by one shower with an age of ~40 Myr. The age distribution of 19 DaG H chondrites differs from that of moderns falls since only three meteorites coincide with the main H chondrite exposure age peak at ~7 Myr, while seven samples show CRE ages <5 Myr. The high fraction of low exposure ages may be due partly to unrecognized pairings. Two H chondrites show evidence of a complex exposure history: i) DaG 908 shows significant neutron-capture ^{36}Cl but only a small amount of neutron-capture ^{41}Ca, indicating a recent change, about 0.15 Myr ago, from a large object to a small object; ii) the exposure history of DaG 904 is less well-constrained, but its cosmogenic nuclide record is best explained with a first-stage exposure on the parent body and a second stage of 1–2 Myr as a relatively large (m-sized) object in space. Low ^{26}Al (and ^{10}Be) concentrations in five other DaG samples with intermediate ^{22}Ne/^{21}Ne ratios seem to indicate that they experienced a more moderate change in size during their exposure history, either due to a breakup event and/or due to the gradual process of space erosion. But, this topic warrants further studies.

Finally, we used the ^{26}Al/^{21}Ne and ^{10}Be/^{21}Ne ratios in 16 DaG meteorites to derive a more reliable equation for the ^{10}Be/^{21}Ne production rate ratio as a function of shielding. The P(^{10}Be)/P(^{21}Ne) ratio seems more dependent on shielding than was predicted by the semi-empirical model of Graf et al. (1990), but much less than was predicted by the purely physical model of Leya et al. (2000).

Acknowledgments–This work was supported by NASA grants NAG5–4992 and NAG5–12846, a LLNL-CAMS grant, and was performed under the auspices of the U.S. DOE by LLNL under contract W-7405-ENG-48. We would like to thank the Max Planck Institut für Chemie in Mainz, the University of Münster, and the University of Freiburg for providing the meteorite samples. This paper benefited from constructive reviews by D. Bogard and, especially, I. Leya. In addition, we are grateful to J. Schlüter for sharing the meteorite location data and satellite images of the DaG region. We also thank Jeff Johnson, Richard Cruz, and George Burr for technical assistance with the sample preparation and AMS measurements of the ^{14}C analyses.

Editorial Handling—Dr. Tim Jull

REFERENCES

Abu Aghreb A. E., Ghadi A. M., Schlüter J., Schultz L., and Thiedig F. 2003. Hamadah al Hamra and Dar al Gani: A comparison of two meteorite fields in the Libyan Sahara (abstract). *Meteoritics & Planetary Science* 38:A48

Albrecht A., Schnabel C., Vogt S., Xue S., Herzog G. F., Begemann F., Weber H. W., Middleton R., Fink D., and Klein J. 2000. Light noble gases and cosmogenic radionuclides in Estherville, Budulan, and other mesosiderites: Implications for exposure histories and production rates. *Meteoritics & Planetary Science* 35:975–986.

Alexeev V. A. 1998. Parent bodies of L and H chondrites: Times of catastrophic events. *Meteoritics & Planetary Science* 33:145–152.

Begemann F., Weber H. W., Vilcsek E., and Hintenberger H. 1976. Rare gases and ^{36}Cl in stony-iron meteorites: Cosmogenic elemental production rates, exposure ages, diffusion losses, and thermal histories. *Geochimica et Cosmochimica Acta* 40:353–368.

Begemann F., Li Z., Schmitt-Strecker S., Weber H. W., and Xu Z. 1985. Noble gases and the history of Jilin meteorite. *Earth and Planetary Science Letters* 72:247–262.

Begemann F., Caiyun F., Weber H. W., and Xianbin W. 1996. Light noble gases in Jilin: More of the same and something new. *Meteoritics & Planetary Science* 31:667–674.

Bland P. A., Berry F. J., Smith T. B., Skinner S. J., and Pillinger C. T. 1996. The flux of meteorites to the Earth and weathering in hot desert ordinary chondrite finds. *Geochimica et Cosmochimica Acta* 60:2053–2059.

Bland P. A., Sexton A. S., Jull A. J. T., Bevan A. W. R., Berry F. J., Thornley D. M., Astin T. R., Britt D. T., and Pillinger C. T. 1998. Climate and rock weathering: A study of terrestrial age dated ordinary chondritic meteorites from hot desert regions. *Geochimica et Cosmochimica Acta* 62:3169–3184.

Bogard D. D. 1995. Impact ages of meteorites: A synthesis. *Meteoritics* 30:244–268.

Cassidy W., Harvey R., Schutt J., Delisle G., and Yanai K. 1992. The meteorite collection sites of Antarctica. *Meteoritics* 27:490–525.

Davis J. C., Proctor I. D., Southon J. R., Caffee M. W., Heikkinen D. W., Roberts M. L., Moore T. L., Turteltaub K. W., Nelson D. E., Loyd D. H., and Vogel J. S. 1990. LLNL/UC AMS facility and research program. *Nuclear Instruments and Methods in Physics Research B* 52:269–272.

Eberhardt P., Eugster O., Geiss J., and Marti K. 1966. Rare gas measurements in 30 stone meteorites. *Zeitschrift für Naturforschung* 21a:414–426.

Eugster O. 1988. Cosmic ray production rates of ^{3}He, ^{21}Ne, ^{38}Ar, ^{83}Kr, and ^{126}Xe in chondrites based on ^{81}Kr-Kr exposure ages. *Geochimica et Cosmochimica Acta* 52:1649–1662.

Eugster O., Michel Th., Niedermann S., Wang D., and Yi W. 1993. The record of cosmogenic, radiogenic, fissiogenic, and trapped noble gases in recently recovered Chinese and other chondrites. *Geochimica et Cosmochimica Acta* 57:1115–1142.

Ferko T. E., Wang M. S., Hillegonds D. J., Lipschutz M. E., Hutchison R., Franks L., Scherer P., Schultz L., Benoit P. H., Sears D. W. G., Singhvi A. K., and Bhandari N. 2002. The irradiation history of the Ghubara (L5) regolith breccia. *Meteoritics & Planetary Science* 37:311–328.

Garrison D. H., Bogard D. D., Albrecht A. A., Vogt S., Herzog G. F., Klein J., Fink D., Dezfouly-Arjomandy B., and Middleton R. 1992. Cosmogenic nuclides in core samples of the Chico L6 chondrite: Evidence for irradiation under high shielding *Meteoritics* 27:371–381.

Gibson E. K. and Bogard D. D. 1978. Chemical alterations of the Holbrook chondrite resulting from terrestrial weathering. *Meteoritics* 13:277–289.

Grady M. M. 2000. *Catalogue of meteorites, 5th edition.* London: The Natural History Museum. 690 p.

Graf T. and Marti K. 1995. Collisional history of H chondrites. *Journal of Geophysical Research—Planets* 100:21247–21263.

Graf T., Baur H., and Signer P. 1990. A model for the production of cosmogenic nuclides in chondrites. *Geochimica et Cosmochimica Acta* 54:2521–2534.

Harvey R. 2003. The origin and significance of Antarctic meteorites. *Chemie der Erde* 63:93–147.

Herzog G. F. and Cressy P. J. 1976. ^{26}Al losses from weathered chondrites. *Meteoritics* 11:59–68.

Herzog G. F., Vogt S., Albrecht A., Xue S., Fink D., Klein J., Middleton R., Weber H. W., and Schultz L. 1997. Complex exposure histories for meteorites with “short” exposure ages. *Meteoritics & Planetary Science* 32:413–422.

Hintenberger H., Schultz L., and Wänke H. 1966. Messung der Diffusionsverluste von radiogenen und spallogenen Edelgasen in Steinmeteoriten II. *Zeitschrift für Naturforschung* 21a:1147–1159.

Huneke J. C., Nyquist L. E., Funk H., Köppel V., and Signer P. 1969. The thermal release of rare gases from separated minerals of the Mocs meteorite. In *Meteorite research,* edited by Millman P. M. Dordrecht: D. Reidel Publishing Company. pp. 901–921.

Huss G. R. 1991. Meteorite mass distributions and differences between Antarctic and non-Antarctic meteorites. *Geochimica et Cosmochimica Acta* 55:105–112.

Jarosewich E. 1990. Chemical analyses of meteorites: A compilation of stony and iron meteorites. *Meteoritics* 25:323–337.

Jull A. J. T., Donahue D. J., and Linick T. W. 1989. Carbon-14 activities in recently fallen meteorites and Antarctic meteorites. *Geochimica et Cosmochimica Acta* 53:2095–2100.

Jull A. J. T., Wlotzka F., Palme H., and Donahue D. J. 1990. Distribution of terrestrial age and petrologic type of meteorites from western Libya. *Geochimica et Cosmochimica Acta* 54: 2895–2898.

Jull A. J. T., Bland P. A., Klandrud S. E., McHargue L. R., Bevan A. W. R., Kring D. A., and Wlotzka F. 2000. Using ^{14}C and ^{14}C-^{10}Be for terrestrial ages of desert meteorites. In *Workshop on extraterrestrial materials from cold and hot deserts,* edited by Schultz L., Franchi I, Reid A., and Zolensky M. LPI Contribution No. 997 Houston: Lunar and Planetary Institute. 99 p.

Jull A. J. T., Koblitz J., Hofmann B., Franchi I. A., McHargue L. R., and Shahab A. 2002. Terrestrial ages of some meteorites from Oman. *Meteoritics & Planetary Science* 37:A74.

Kring D. A., Jull A. J. T., McHargue L. R., Bland P. A., Hill D. H., and Berry F. J. 2001. Gold Basin meteorite strewn field, Mojave Desert: Relict of a small Late Pleistocene impact event. *Meteoritics & Planetary Science* 36:1057–1066.

Leya I. and Michel R. 1998. Modeling the cosmic ray record of the iron meteoroid Grant (abstract #1172). 29th Lunar and Planetary Science Conference. CD-ROM.

Leya I., Lange H. J., Neumann S., Wieler R., and Michel R. 2000. The production of cosmogenic nuclides in stony meteoroids by galactic cosmic ray particles. *Meteoritics & Planetary Science* 35:259–286.

Leya I., Wieler R., Aggrey K., Herzog G. F., Schnabel C., Metzler K., Hildebrand A. R., Bouchard M., Jull A. J. T., Andrews H. R., Wang M. S., Ferko T. E., Lipschutz M. E., Wacker J. F., Neuman S., and Michel R. 2001. Exposure history of the St-Robert (H5) fall. *Meteoritics & Planetary Science* 36:1479–1494.

Marti K. 1967. Trapped xenon and the classification of chondrites. *Earth and Planetary Science Letters* 2:193–196.

Masarik J. and Reedy R. C. 1994. Effects of bulk composition on nuclide production processes in meteorites. *Geochimica et Cosmochimica Acta* 58:5307–5317.

Masarik J., Nishiizumi K., and Reedy R. C. 2001. Production rates of cosmogenic helium-3, neon-21, and neon-22 in ordinary chondrites and the lunar surface. *Meteoritics & Planetary Science* 36:643–650.

Nagai H., Honda M., Imamura M., and Kobayashi K. 1993. Cosmogenic ^{10}Be and ^{26}Al in metal, carbon, and silicate of meteorites. *Geochimica et Cosmochimica Acta* 57:3705–3723.

Nishiizumi K. Forthcoming. Preparation of ^{26}Al AMS standards. In *Proceedings of the 9th international symposium on accelerator mass spectrometry. Nuclear Instruments & Methods.*

Nishiizumi K., Regnier S., and Marti K. 1980. Cosmic ray exposure ages of chondrites, pre-irradiation, and constancy of cosmic ray flux in the past. *Earth and Planetary Science Letters* 56:156–170.

Nishiizumi K., Elmore D., Ma X. Z., and Arnold J. R. 1984. ^{10}Be and ^{26}Al depth profiles in an Apollo 15 drill core. *Earth and Planetary Science Letters* 70:157–163.

Nishiizumi K., Caffee M. W., and Jull A. J. T. 1998. Exposure histories of Dar al Gani 262 lunar meteorite (abstract #1957). 29th Lunar and Planetary Science Conference. CD-ROM.

Nishiizumi K., Caffee M. W., and DePaolo D. J. 2000. Preparation of ^{41}Ca AMS standards. *Nuclear Instruments & Methods* B172: 399–403.

Nishiizumi K., Caffee M. W., Jull A. J. T., and Klandrud S. E. 2001a. Exposure histories of shergottites Dar al Gani 476/487/670/735 and Sayh al Uhaymir 005 (abstract #2117). 32nd Lunar and Planetary Science Conference. CD-ROM.

Nishiizumi K. and Caffee M. W. 2001b. Exposure histories of lunar meteorites Dhofar 025, 026, and Northwest Africa 482. *Meteoritics & Planetary Science* 36:A148–149.

Nishiizumi K., Okazaki R., Park J., Nagao K., Masarik J., and Finkel R. C. 2002. Exposure and terrestrial histories of Dhofar 019 martian meteorite (abstract #1366). 33rd Lunar and Planetary Science Conference. CD-ROM.

Patzer A., Scherer P., Weber H. W., and Schultz L. 1999. New exposure ages of chondrites: Short transfer times from asteroid belt to Earth? (abstract #1145). 30th Lunar and Planetary Science Conference. CD-ROM.

Scherer P., Schultz L., and Loeken T. 1994. Weathering and atmospheric noble gases in chondrites. In *Noble gas geochemistry and cosmochemistry,* edited by Matsuda J. Tokyo: Terra Scientific Publishing Company. pp. 43–53.

Scherer P., Herrmann S., and Schultz L. 1998. Noble gases in twenty-one Saharan LL chondrites: Exposure ages and possible pairings. *Meteoritics & Planetary Science* 33:259–265.

Scherer P., Pätsch M., and Schultz L. 2000. Noble gases in 15 meteorites from the Sahara: Eucrites, ureilites, and ordinary chondrites. In *Workshop on extraterrestrial materials from cold and hot ceserts,* edited by Schultz L., Franchi I, Reid A., and Zolensky M. LPI Contribution No. 997. Houston: Lunar and Planetary Institute. 99 p.

Schlüter J., Schultz L., Thiedig F., Al-Mahdi B. O., and Abu Aghreb A. E. 2002. The Dar al Gani meteorite field (Libyan Sahara): Geological setting, pairing of meteorites, and recovery density. *Meteoritics & Planetary Science* 37:1079–1093.

Schmitz B., Tassinari M., and Peucker-Ehrenbrink B. 2001. A rain of ordinary chondritic meteorites in the early Ordovician. *Earth and Planetary Science Letters* 194:1–15.

Schultz L. and Stöffler D. 1993. Shock effects and noble gas concentrations in chondrites (abstract). *Meteoritics* 28:432.

Schultz L., Weber H. W., and Begemann F. 1990. Planetary noble gases in H3 and H4 chondrite falls. *Meteoritics* 25:405–406.

Schultz L., Weber H. W., and Begemann F. 1991. Noble gases in H chondrites and potential differences between Antarctic and non-Antarctic meteorites. *Geochimica et Cosmochimica Acta* 55:59–66.

Sharma P., Kubik P. W., Fehn U., Gove G. E., Nishiizumi K., and Elmore D. 1990. Development of ^{36}Cl standards for AMS. *Nuclear Instruments & Methods* B52:410–415.

Stelzner T. Heide K., Bischoff A., Weber D., Scherer P. Schultz L., Happel., Schrön W., Neupert U., Michel R., Clayton R. N., Mayeda T. K., Bonani G., Haidas I., Ivy-Ochs S., and Suter M. 1999. An interdisciplinary study of weathering effects in ordinary chondrites from the Acfer region, Algeria. *Meteoritics & Planetary Science* 34:787–794.

Stöffler D., Keil K., and Scott E. R. D. 1991. Shock metamorphism of ordinary chondrites. *Geochimica et Cosmochimica Acta* 54: 3845–3867.

Vogt S., Fink D., Klein J., Middleton R., Dockhorn B., Korschinek G., Nolte E., and Herzog G. F. 1991. Exposure histories of the lunar meteorites: MAC 88104, MAC 88105, Y-791197, and Y-86032. *Geochimica et Cosmochimica Acta* 55:3157–3166.

Wasson J. T. and Kallemeyn G. W. 1988. Composition of chondrites. *Philosophical Transactions of the Royal Society of London A* 325:535–544.

Wasson J. T. and Wang S. 1991. The histories of ordinary chondrite parent bodies: U,Th-He age distributions. *Meteoritics* 26:161–167.

Welten K. C. 1999. Concentrations of siderophile elements in nonmagnetic fractions of Antarctic H and L chondrites: A quantitative approach to weathering effects. *Meteoritics & Planetary Science* 34:259–270.

Welten K. C., Nishiizumi K., Caffee M. W., Schäfer J., and Wieler R. 1999. Terrestrial ages and exposure ages of Antarctic H chondrites from Frontier Mountain, North Victoria Land. *Antarctic Meteorite Research* 12:94–107.

Welten K. C., Nishiizumi K., Masarik J., Caffee M. W., Jull A. J. T., Klandrud S. E., and Wieler R. 2001. Cosmic ray exposure history of two Frontier Mountain H chondrite showers from spallation and neutron-capture products. *Meteoritics & Planetary Science* 36:301–317.

Welten K. C., Caffee M. W., Leya I., Masarik J., Nishiizumi K., and Wieler R. 2003. Noble gases and cosmogenic radionuclides in the Gold Basin L4 chondrite shower: Thermal history, exposure history, and pre-atmospheric size. *Meteoritics & Planetary Science* 38:157–173.

Wieler R., Baur H., Pedroni A., Signer P., and Pellas P. 1989. Exposure history of the regolithic chondrite Fayetteville: I. Solar-gas-rich matrix. *Geochimica et Cosmochimica Acta* 53:1441–1448.

Wlotzka F. 1993. A weathering scale for the ordinary chondrites. *Meteoritics* 28:460.